DTU Physics
Department of Physics

Bachelor Thesis

Modeling of Concentration Polarisation in Electrokinetic Microsystems

Jacob Søberg Bach
s113069

Emil Launtoft Pedersen
s113085

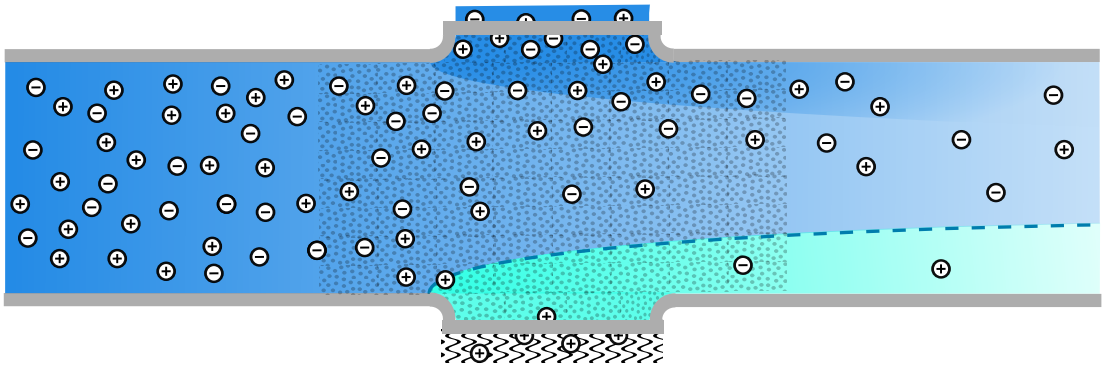

Supervisor: Henrik Bruus

Department of Physics
Technical University of Denmark

23 June 2014

Front page illustration shows a device with porous medium in the middle to effectively form many microchannels. We shall study this device in the end of this thesis.

Abstract

In this thesis we present a way to model a desalination device motivated by the electrokinetic behavior in microscale systems. Many analytical and numerical studies have already been carried out for microchannel systems but the channel size makes them unprofitable or maybe even impossible to produce and sell. We therefore suggest device with a larger channel size with a porous medium to effectively form many microchannel. Scaling up from micrometre to e.g. millimetre is not straight forward as many phenomenons in the microchannel does not scaled linear with the size of the channel.
We derive analytical and numerical solution for a simple straight microchannel with a cation selective membrane in order to understand the basic behaviour of electrolytes in a microchannel under the influence of an external electrical potential. We investigate the concepts of overlimiting current and depletion. The knowledge from the microchannel will then be used to develop a reliable model for the porous material by averaging some of the electrokinetic phenomenons measured on the small scale.
For the new model we see some of the same behaviours for the overlimiting current and the depletion region induced by the porosity as we saw for the microchannel. We find that numerical results for depletion and overlimiting current can be partly described by analytical expression from the microchannel. Numerical issues have made it difficult to understand the whole system and some aspects have not been possible to simulate. We have however been able to make decent analysis of the relation between flow and overlimiting current.

Resumé

I denne afhandling præsenterer vi en måde at modellere en afsaltningsenhed, motiveret af elektrokinetiske effekter i mikrosystemer. Flere analytiske og numeriske undersøgelser er allerede udført for mikrokanalsystemer, men kanalstørrelsen gør dem urentable eller ligefrem umulige at producere og sælge. Derfor foreslår vi en enhed med en større kanalstørrelse indeholende et porøst medium til effektivt at forme mange mikrokanaler. At skalere op fra mikrometer til millimeter er ikke lige til, da mange fænomener i mikrokanalen ikke skalerer linæert med forstørrelsen af kanalaen.
Vi udleder analytiske og numeriske løsninger for en simpel lige mikrokanal med en kation selektiv membran, for at være i stand til at forstå den basale opførsel af elektrolytter i en mikrokanal under indflydelse af en ekstern elektrisk potential.
Vi undersøger koncepterne overbegrænsende strøm og ion-udtømning. Viden fra mikrokanalen vil blive brugt til at udvikle en troværdig model for det porøse materiale ved at midle elektrokinetiske fænomener målt på mikroskala.
For den nye model ser vi nogle af de samme opførsler for den overbrænsende strøm og udtøminingregionen, introduceret af porøsiteten, som vi så i mikrokanalen. Vi finder ud af, at numeriske resultater for udtrømning og den overbegrænsende strøm delvist kan beskrives af de analytiske udtryk fra mikrokanalen. Numeriske problemer har gjort det svært at forstå hele systemet og nolge aspekter har ikke været mulige at simulere. Vi har dog alligevel været i stand til at lave gode analysere af relationen mellem strømninger og den overbegrænsende strøm.

Preface

This thesis is submitted as fulfillment of the prerequisites for obtaining the B.Sc. in Physics and Nanotechnology degree from the Technical University of Denmark. The work has been carried out from February to June 2014 at the Department of Micro- and Nanotechnology (DTU Nanotech) in the Theoretical Microfluidics Group (TMF) headed by professor Henrik Bruus. The project covers 20 ECTS points each. We will like to thank several people for help and support during this project. First of all we will thank our supervisor Henrik Bruus both for the many meetings giving us a great insight in the exiting field of microfluidcs, but also for discussing the approach to theoretical physics in general. We will also thank our co-supervisor Christoffer P. Nielsen for comprehensive explanations and not least for introducing us to COMSOL. Finally we will thank the TMF group for providing a valuable working environment during the project and for including us in social group events in a good way.

Due to requirements from the Danish Ministry of Education we are required to inform who is responsible for which parts of the thesis. Jacob is responsible for all all odd pages and Emil is responsible all even pages.

Jacob Søberg Bach

Emil Launtoft Pedersen

Department of Physics
Technical University of Denmark
23 June 2014

Contents

List of Figures

List of Tables

List of symbols

Symbol	Description	Unit
c_i	Concentration of species i	m^{-3}
c^{i}	Interstitial concentration	m^{-3}
c^{s}	Superficial concentration	m^{-3}
d_{hyd}	Hydraulic diameter	m
d_{e}	Height of extensions	m
$\boldsymbol{D}$	Electric displacement	$\mathrm{C\ m}^{-2}$
D_i	Diffusivity of chemical species i	$\mathrm{C\ m}^2\ \mathrm{s}^{-1}$
$\boldsymbol{E}$	Electrical field	$\mathrm{V\ m}^{-1}$
e	The elementary charge	1.602×10^{-19} C
$\boldsymbol{f}$	Body force density	$\mathrm{N\ m}^{-3}$
H	Height of channel	m
$\boldsymbol{J}_i$	Ion current of chemical species i	$\mathrm{m}^{-2}\ \mathrm{s}^{-1}$
k	Permeability in porous medium	m^2
k_{B}	Boltzmann constant	$1.38 \times 10^{-23}\mathrm{J\ K}^{-1}$
K	Kozeny constant	
L	Length of channel	m
M	Mass	kg
p	Pressure	$\mathrm{N\ m}^{-2}$
Q	Volume flow rate	$\mathrm{m}^3\ \mathrm{s}^{-1}$
Re	Reynolds number	
S	Specific area	m^{-1}
T	Temperature	K
$\boldsymbol{v}$	Velocity vector	$\mathrm{m\ s}^{-1}$
$\boldsymbol{v}^{\mathrm{i}}$	Interstitial velocity vector	$\mathrm{m\ s}^{-1}$
$\boldsymbol{v}^{\mathrm{s}}$	Superficial velocity vector	$\mathrm{m\ s}^{-1}$
v	Velocity	$\mathrm{m\ s}^{-1}$
v^{i}	Interstitial velocity	$\mathrm{m\ s}^{-1}$
v^{s}	Superficial velocity	$\mathrm{m\ s}^{-1}$
V_{T}	Thermal voltage	mV
W_{m}	Width of membrane	m
W_{p}	Width of porous medium	m
Z	Valence number	
ϵ_0	Vacuum permittivity	$8.85 \times 10^{-12}\mathrm{F\ m}^{-1}$
ϵ_{w}	Permittivity of water	$80.1\ \epsilon_0$
ϵ_{g}	Permittivity of glass	$2\ \epsilon_0$
ε_{p}	Porosity	

Symbol	Description	Unit
ζ	Zeta-potential	V
η	Dynamic viscosity	N m^{-2} s
λ_D	The Debye length	m
μ_i	Mobility of chemical species i	m^2 s^{-1} V^{-1}
ρ	Mass density	kg m^{-3}
ρ^{i}	Interstitial mass density	kg m^{-3}
ρ^{s}	Superficial mass density	kg m^{-3}
σ	Surface charge per area	C m^{-2}
$\boldsymbol{\sigma}$	Viscous stress tensor	N m^{-2}
τ	Tortuosity	
ϕ	Electric potential	V
$\boldsymbol{\nabla}$	Gradient or nabla operator	
$\boldsymbol{\nabla}\cdot$	Divergent operator	
∇^2	Laplace operator	
δ	Kronecker delta	
$\boldsymbol{\Gamma}$	Flux	
$\mathcal{L}$	Differential operator	
Ω	Computational domain	
$\partial\Omega$	Domain boundary	
ψ_n	Basis functions	
$C(g)$	Relative convergence parameter	
d_{mesh}	Mesh size	
g_n	Test function	
F	Source term	
$\boldsymbol{n}$	Surface outward normal vector	
$\langle\cdot\rangle$	Averaged	
$\langle\cdot,\cdot\rangle$	Inner product	

1 Introduction

Pure drinking water is an important necessity for all life on earth. Around 97 % of earth's water is sea water with high ionic concentration[1]. Thus desalination of sea water suggests a purposeful method for water supply in stressed regions. In this thesis we investigate electrokinetic effects applicable in the scope of desalination. We will study the microchannel with a cation selective membrane studied by the group of Henrik Bruus, DTU[2] and the group of Martin Bazant, MIT[3, 4]. Based on this study we investigate a device for desalination using porous medium to effectively form several microchannels.

1.1 Weak solutions and the ideal gas approximation

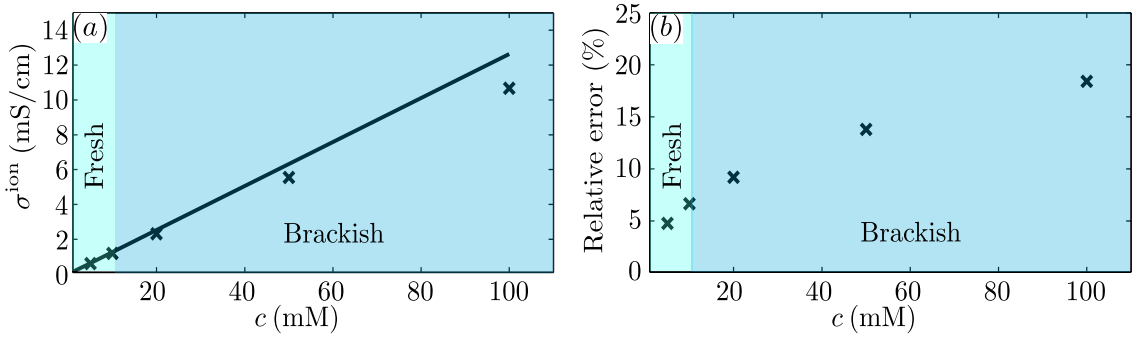

Figure 1.1: Relation between ionic conductance σ^{ion} and concentration c. (a) Solid line shows the ideal gas approximation where we have used $\mu^{\text{ion}}_{Na^+} = 5.19 \times 10^{-1}\ \text{m}^2\,(\text{V s})^{-1}$ and $\mu^{\text{ion}}_{Cl^-} = 7.91 \times 10^{-1}\ \text{m}^2\,(\text{V s})^{-1}$ at 25°C[5]. The crosses are experimental values[6]. (b) The relative error between the ideal gas approximation and the experimental values. The colors mark different salinity regions where we define freshwater as 0.5 ppt or around 9 mM for NaCl[7].

Desalination of sea water might not be carried out by only one process. In this thesis we shall work with desalination of weak solutions with an ionic concentration lower than 50 mM i.e. weaker than sea water which is around 600 mM[8]. One great advantage when working with weak solutions is that we can consider the ions as non-interacting and thus apply an ideal gas approximation. This is shown in Fig. 1.1(a) where we compare

experimental values for ionic conductivity with the value calculated in the ideal gas approximation. In the ideal gas approximation the ionic conductance for many particles is simply the sum of each particles conductance. In Fig. 1.1(b) we show that for solutions stronger than 50 mM this approximation begins to fail due to particle interaction.

1.2 The continuum hypothesis

When dealing with fluids, e.g. liquids and gasses, the first important thing we need to establish is the conceptual model. How do we consider fluids? We know that fluids consist of molecules and thus are quantized in length scales of the intermolecular distances in the order of 3 nm for gasses and 0.3 nm for liquids. However keeping track of every single particle is obviously practically impossible. Therefore, what we do in this thesis is we apply the everyday intuition and consider a fluid as perfectly continuous i.e. not consisting of molecules and empty space but completely filling the space it occupies. This is what is stated in the continuum hypotheses. This enables us to describe all quantities of the fluid in terms of continuous fields defined in every point $\boldsymbol{r}$.
Now the natural question to ask is what value should we ascribe to e.g. a scalar field in a given position $\boldsymbol{r}$? This question leads to the concept of a fluid particle which we define as a small volume $\mathcal{V}$ centered at the position $\boldsymbol{r}$. The value of e.g. a scalar field in the position $\boldsymbol{r}$ at a time t is then determined by the particles contained in a small fluid particle around $\boldsymbol{r}$ at a time t. Three examples are density $\rho(\boldsymbol{r}, t)$, velocity $\boldsymbol{v}(r, t)$ and then momentum $\boldsymbol{P}(\boldsymbol{r}, t)$,

$$\rho(\boldsymbol{r}, t) \equiv \frac{1}{\mathcal{V}} \sum_{i \in \mathcal{V}} m_i, \tag{1.1a}$$

$$\boldsymbol{v}(\boldsymbol{r}, t) \equiv \frac{1}{\rho(\boldsymbol{r}, t)\mathcal{V}} \sum_{i \in \mathcal{V}} m_i \boldsymbol{v}_i, \tag{1.1b}$$

$$\boldsymbol{P}(\boldsymbol{r}, t) = \rho(\boldsymbol{r}, t)\boldsymbol{v}(\boldsymbol{r}, t) = \frac{1}{\mathcal{V}} \sum_{i \in \mathcal{V}} m_i \boldsymbol{v}_i. \tag{1.1c}$$

Note that we have chosen the Eulerian description where $\boldsymbol{r}$ is fixed, i.e. *not* dependent of t. To avoid cluttered notation we will whenever unnecessary omit the dependencies and write ρ instead of $\rho(\boldsymbol{r}, t)$, $\boldsymbol{v}$ instead of $\boldsymbol{v}(\boldsymbol{r}, t)$ and so forth.
We can give an estimation of the minimum scale where the continuum hypothesis is valid by considering the size of the fluid particle. On one hand we want to make it so small as possible to be able to describe small spatial variations in the fields. On the other hand we need it to be large enough to avoid microscopic fluctuations. We choose a characteristic length λ^* of the fluid particle so that its volume is $\mathcal{V} = (\lambda^*)^3$. The number of molecules N inside this volume can be considered as uncorrelated random events, i.e. following a Poisson distribution with the relative uncertainty $\sqrt{N}/N$[5]. If we require a relative uncertainty of 0.5% and use the average distance $\lambda \approx 0.3$ nm between molecules in a liquid, we need $N = 4 \times 10^4$ molecules corresponding to $\lambda^* = \lambda N^{1/3} \approx 10$ nm. This determines the size of a fluid particle. Thus for systems with length scales much larger than λ^* the continuum

hypothesis is assumed valid. In this thesis we mainly work with length scales from 10^{-6} m to 10^{-3} m. However, the Debye length introduced in chapter Chapter 3 is in the order of 10 nm for our systems, and thus results related to the Debye length should be treated with care. We emphasize that mathematically we shrink down the fluid particle to zero size and consider all fields as well-defined in all points $\boldsymbol{r}$. Thus the size of the fluid particle only provides a length scale to helps us validating our physical model.

1.3 Brief overview

Chapter 2 - Governing Equations We present the governing equations covering hydrodynamics, electrostatics, electrokinetics and thermodynamics.

Chapter 3 - Electrolyte near charged wall We study the behavior of an electrolyte near a charged wall introducing the concepts of the screening layer and the Debye length.

Chapter 4 - Numerical modeling We give a brief introduction to the finite element method used by COMSOL and we introduce the weak formulation of conservation equations.

Chapter 5 - Microchannel We investigate a microchannel with negatively charged walls and a cation selective membrane. We introduce the concepts of overlimiting current, depletion region and charge polarization. A linear correspondence between the size of the depletion region and the channel length motivates a system on a larger scale.

Chapter 6 - Modeling of porous medium We present how we adjust the governing equations for hydrodynamics and electrokinetics when dealing with porous medium. Physical properties of the porous medium are described by the parameters porosity ε_{p}, tortuosity τ and specific area S.

Chapter 7 - Desalination Motivated by the electrokinetic behavior of the microchannel we suggest a device for desalination on a larger scale using porous medium to effectively form many microchannels. The system reveals some of the same behaviors as the microchannel and we show the occurrence of a depletion region and overlimiting current. We investigate the effect of transverse pressure driven flow and show a correspondence between the limiting current and the pressure drop.

2 | Governing Equations

In this chapter we present the general physics we shall use in this thesis. The important topics are hydrodynamics, electrostatics, electrodynamics and thermodynamics. In Chapter 6 we adjust some of these governing equations to model porous medium.

2.1 Hydrodynamics

Consider a fixed arbitrary volume Ω in a fluid through which fluid is able to flow freely. We exploit conservation of mass M_Ω inside Ω so that the change of mass $\partial_t M_\Omega$ must be due to advection of mass into Ω,

$$\partial_t M_\Omega = \partial_t \int_\Omega \mathrm{d}\boldsymbol{r}\ \rho = \int_\Omega \mathrm{d}\boldsymbol{r}\ \partial_t \rho = \int_{\partial\Omega} \mathrm{da}\ (-\boldsymbol{n})\cdot(\rho\boldsymbol{v}) = \int_\Omega \mathrm{d}\boldsymbol{r}\ (-\boldsymbol{\nabla})\cdot(\rho\boldsymbol{v}), \tag{2.1}$$

where in the last step we have used Gauss's divergence theorem. Note that the second step is only legal since Ω is *fixed*. Since Eq. (2.1) holds for *any* Ω the integrands in the third and last part must be equal so that we get the continuity equation Eq. (2.2a) which reduces to Eq. (2.2b) for incompressible fluids,

$$\partial_t \rho = -\boldsymbol{\nabla}\cdot(\rho\boldsymbol{v}), \tag{2.2a}$$

$$0 = \boldsymbol{\nabla}\cdot\boldsymbol{v} \quad \text{(incompressible fluids)}, \tag{2.2b}$$

where ρ is constant in space and time. This was an example of establishing a conservation equation, in this case for mass.
In the same way we now consider the conservation of momentum inside Ω. The change of momentum inside Ω must be due to either advection of momentum into Ω, stress forces (pressure, viscosity) on the surface of Ω or bodyforces (gravitational, electric) on the bulk of Ω. Thus in analogy with Eq. (2.2a),

$$\partial_t (\rho\boldsymbol{v}) = -\boldsymbol{\nabla}\cdot[(\rho\boldsymbol{v})\,\boldsymbol{v} - \boldsymbol{\sigma}] + \boldsymbol{f}^{\mathrm{body}}, \tag{2.3}$$

where $\boldsymbol{\sigma}$ is the second order viscous stress tensor which we define as

$$\sigma_{ij} = -p\delta_{ij} + \eta\,(\partial_i v_j + \partial_j v_i) + (\beta - 1)\,\eta\,(\partial_k v_k)\,\delta_{ij}, \tag{2.4a}$$

$$\sigma_{ij} = -p\delta_{ij} + \eta\,(\partial_i v_j + \partial_j v_i) \quad \text{(incompressible fluids)}. \tag{2.4b}$$

Here p is the pressure, η is the dynamic viscosity describing internal friction due to shear stress, and β is the dimensionless viscousity ratio describing the internal friction due to compression. δ_{ij} is the Kronecker delta. For incompressible fluids $\partial_k v_k \equiv \boldsymbol{\nabla} \cdot \boldsymbol{v} = 0$ accoding to Eq. (2.2b) so that Eq. (2.4a) reduces to Eq. (2.4b).

Combining Eqs. (2.2a), (2.3) and (2.4b), we write the Navier-Stokes equation,

$$\rho \left[\partial_t + \boldsymbol{v}\cdot\boldsymbol{\nabla}\right] \boldsymbol{v} = -\boldsymbol{\nabla} p + \eta \nabla^2 \boldsymbol{v} + \boldsymbol{f}^{\text{body}}. \tag{2.5}$$

As seen, the Navier-Stokes equation is nonlinear due to the term inertia $\rho(\boldsymbol{v}\cdot\boldsymbol{\nabla})\boldsymbol{v}$. However this term might be neglected under certain conditions as follows:

We write the Navier-Stokes equation in dimensionless form by introducing the dimensionless variables $\tilde{\boldsymbol{r}} = \dfrac{\boldsymbol{r}}{L_0}$, $\tilde{\boldsymbol{v}} = \dfrac{\boldsymbol{v}}{v_0}$, $\tilde{t} = \dfrac{t}{T_0}$, $\tilde{p} = \dfrac{p}{P_0}$, where L_0, v_0, T_0 and P_0 are characteristic scaling variables for the system. We chose the intrinsic time scale for the system, $T_0 = \dfrac{L_0}{v_0}$ and then $P_0 = \dfrac{v_0 \eta}{L_0}$ to get the Navier-Stokes equation in dimensionless form (neglecting body forces),

$$\frac{L_0 \rho v_0}{\eta} \left[\partial_{\tilde{t}} + \tilde{\boldsymbol{v}}\cdot\tilde{\boldsymbol{\nabla}}\right] \tilde{\boldsymbol{v}} = -\tilde{\boldsymbol{\nabla}}\tilde{p} + \tilde{\nabla}^2 \tilde{\boldsymbol{v}}, \tag{2.6}$$

where $\tilde{\boldsymbol{\nabla}} = L_0 \boldsymbol{\nabla}$ is the spatial derivative with respect to the dimensionless position $\tilde{\boldsymbol{r}}$. Here $Re \equiv \dfrac{L_0 \rho v_0}{\eta}$ is the Reynold's number. If $Re \ll 1$ we see that the viscous term $\tilde{\nabla}^2 \tilde{\boldsymbol{v}}$ dominates and the nonlinear inertia term $(\tilde{\boldsymbol{v}}\cdot\tilde{\boldsymbol{\nabla}})\tilde{\boldsymbol{v}}$ vanishes. In this thesis we consider water with $\rho_{\text{w}} \approx 10^3$ kg m^{-3}, $\eta_{\text{w}} \approx 10^{-3}$ Pa s and micro systems with $L_0 \approx 10^{-6}$ m and velocities in the order of $v_0 \approx 10^{-4}$ m s^{-1}, which yields $Re \approx 10^{-4}$ so that the inertia term is vanishing. Furthermore if we assume steady state ($\partial_{\tilde{t}} \tilde{\boldsymbol{v}} = 0$) the Navier-Stokes equation reduces to the linear Stokes equation,

$$\boldsymbol{0} = -\boldsymbol{\nabla} p + \eta \nabla^2 \boldsymbol{v} + \boldsymbol{f}^{\text{body}} \quad \text{for } Re \ll 1 \text{ and steady state.} \tag{2.7}$$

Note however, that the requirement $Re \ll 1$ for Eq. (2.7) to be valid is less necessary for systems with high symmetry, where $(\boldsymbol{v}\cdot\boldsymbol{\nabla})\boldsymbol{v}$ is vanishing as we shall see in Chapters 5 and 7 where we model straight channels.

2.1.1 Hydrodynamics in porous media

An important part of this thesis is the introduction of porous medium. To model the flow in the porous medium we apply Darcy's law,

$$\boldsymbol{0} = -\boldsymbol{\nabla} p - \frac{\eta}{k}\boldsymbol{v}, \tag{2.8}$$

where k is the permeability with dimensions of length squared. Darcy's law arise from considering the porous medium as consisting of many micro channels. The important simplification in Darcy's law is that the term $-\dfrac{\eta}{k}\boldsymbol{v}$ accounts for all viscous drag from the

porous medium so that we do not have to calculate $\eta\nabla^2\boldsymbol{v}$ for every single channel. Hence Darcy's law do not give the correct velocity profile in each single channel, but it gives the correct flow, provided k is chosen appropriately. How to choose k depends on the specific model which we describe in Chapter 6.

If the porous medium is placed in a channel we still need the term $\eta\boldsymbol{\nabla}^2\boldsymbol{v}$ to account for the viscosity from the walls. In this case we apply the usual Navier-Stokes equation with the extra term from Darcy's law,

$$\rho\left[\partial_t + \boldsymbol{v}\cdot\boldsymbol{\nabla}\right]\boldsymbol{v} = -\boldsymbol{\nabla}p + \eta\nabla^2\boldsymbol{v} + \boldsymbol{f}^{\text{body}} - \frac{\eta}{k}\boldsymbol{v}. \tag{2.9}$$

2.2 Electrostatics

In this thesis we apply Gauss's law for the electric displacement field $\boldsymbol{D}$,

$$\boldsymbol{\nabla}\cdot\boldsymbol{D} = \rho_{\text{el}}, \tag{2.10}$$

where ρ_{el} is the charge density.

We shall only work with linear media with no directional preference of polarization, so that the electric field $\boldsymbol{E}$ is parallel to $\boldsymbol{D}$ through the relation $\boldsymbol{D} = \epsilon\boldsymbol{E}$, where ϵ is the scalar permittivity expressible in terms of the relative permittivity ϵ_r times the vacuum permittivity ϵ_0, $\epsilon = \epsilon_r\epsilon_0$. We emphasize that when working with inhomogeneous media the permittivity can be dependent of posoition. For linear media we write Gauss's law for the electric field,

$$\boldsymbol{\nabla}\cdot(\epsilon(\boldsymbol{r})\boldsymbol{E}) = \rho_{\text{el}} \quad \text{(generally)}, \tag{2.11a}$$

$$\boldsymbol{\nabla}\cdot\boldsymbol{E} = \frac{\rho_{\text{el}}}{\epsilon} \quad \text{(linear media)} \tag{2.11b}$$

According to Maxwell-Faraday's law, $\boldsymbol{\nabla}\times\boldsymbol{E} = -\partial_t\boldsymbol{B}$, where $\boldsymbol{B}$ is the magnetic field. Thus for no magnetic field or for slowly time varying magnetic field, $\boldsymbol{E}$ has zero curl and is therefore a conservative vector field. I.e. there exists a scalar electric potential ϕ for $\boldsymbol{E}$ such that

$$\boldsymbol{E} = -\boldsymbol{\nabla}\phi. \tag{2.12}$$

Note that the minus sign arises since we want ϕ to be the electric potential defined as the energy it takes to move a unit charge from a reference point $\mathcal{O}$ (with reference potential $\phi(\mathcal{O}) \equiv 0$ V) through any path (since $\boldsymbol{E}$ is conservative) to a position $\boldsymbol{r}$,

$$\phi(\boldsymbol{r}) \equiv -\int_{\mathcal{O}}^{\boldsymbol{r}} \mathrm{d}\boldsymbol{l}\cdot\boldsymbol{E}(\boldsymbol{r}). \tag{2.13}$$

Combining Eqs. (2.11) and (2.12) we reach the Poisson equation relating the electric potential ϕ and the charge density ρ_{el},

$$\boldsymbol{\nabla}\cdot(\epsilon(\boldsymbol{r})\boldsymbol{\nabla}\phi) = -\rho_{\text{el}} \quad \text{(generally)}, \tag{2.14a}$$

$$\boldsymbol{\nabla}^2\phi = -\frac{\rho_{\text{el}}}{\epsilon} \quad \text{(homogeneous media)}. \tag{2.14b}$$

2.3 Electrokinetics

Just as for mass and momentum, also the concentration of ions $c_\pm$ is conserved, provided that no chemical reactions R occur. Thus we can state a conservation equation of the the same form as the continuity equations of mass Eq. (2.2),

$$\partial_t c_\pm = -\boldsymbol{\nabla}\cdot\boldsymbol{J}_\pm + R \tag{2.15a}$$

$$0 = -\boldsymbol{\nabla}\cdot\boldsymbol{J}_\pm \quad \text{(stady state and no chemical reactions).} \tag{2.15b}$$

where $\boldsymbol{J}_\pm$ is the ion current defined as the number of positie/negative ions $c_\pm$ passing through a unit area per unit time. Througout this thesis we shall assume no chemical reactions so that Eq. (2.15b) is valid. The ion current $\boldsymbol{J}_\pm$ can be described by adding up contributions from advection, diffusion and electrophoresis,

$$\boldsymbol{J}_\pm = \boldsymbol{J}_\pm^{\text{adv}} + \boldsymbol{J}_\pm^{\text{diff}} + \boldsymbol{J}_\pm^{\text{elec}}. \tag{2.16}$$

The advection term simply expresses that the ions follow the flow of the fluid that surrounds them, $\boldsymbol{J}_\pm^{\text{adv}} = c_\pm \boldsymbol{v}$.

The diffusion term expresses the statistical fact that if many particles fluctuate randomly, they will distribute evenly over the entire domain. So due to probability the net flow of particles will be from high concentration to low. A linear model of this behavior is given by Fick's law,

$$\boldsymbol{J}_\pm^{\text{diff}} = -D_\pm \boldsymbol{\nabla} c_\pm, \tag{2.17}$$

where $D_\pm$ is the diffusivity of positive and negative ions respectively. Note that ficks law has noting to do with particle interaction and therefore the diffusion of positive ions is only governed by the concentration of positive ions, and not the concentration of all particles.

Finally the electrophoresis term expresses the ion current density due to the presence of an electric field. An ion with charge $\pm|Z|e$, where Z is the valence number, will be accelerated by the electric field until it reaches a constant drift velocity balanced by the stokes drag. The ionic mobility $\mu_\pm^{\text{ion}}$ of the particle relates this electrophoretic velocity $\boldsymbol{v}_{\text{ep}}$ and the electric field through $\boldsymbol{v}_{\text{ep}} = \mu_\pm^{\text{ion}} \boldsymbol{E}$. Thus, the ion current can be written

$$\boldsymbol{J}_\pm^{\text{elec}} = c_\pm \boldsymbol{v}_{\text{ep}} = c_\pm \mu_\pm^{\text{ion}} \boldsymbol{E} = -c_\pm \mu_\pm^{\text{ion}} \boldsymbol{\nabla}\phi, \tag{2.18}$$

where we have applied the ideal gas approximation for weak solutions and assumed no particle interaction so that the mobility of N ions is simply $N\mu_\pm^{\text{ion}}$. We finally write the full Nernst-Planck equation by using the Einstein relation for the diffusivity $D_\pm = \pm\mu_\pm^{\text{ion}} V_{\text{T}}$, where we have introduced the thermal voltage, $V_{\text{T}} = k_{\text{B}}T/|Z|e$,

$$\boldsymbol{J}_\pm = c_\pm \boldsymbol{v} - D_\pm \boldsymbol{\nabla} c_\pm \mp c_\pm D_\pm V_{\text{T}}^{-1} \boldsymbol{\nabla}\phi. \tag{2.19}$$

2.4 Thermodynamics

To understand how charged particles in an electrolyte distribute in the presence of an electric field it is advantageous to consider the electrochemical potential. As discussed in

the introduction, we shall assume weak solutions lower than 50 mM. It is well known[5] that ions in weak solutions can be modeled as non interacting particles. Hence we adopt the approach from the ideal gas, where the chemical potential for positive or negative particles $\mu_\pm$ has a logarithmic dependency on the concentration of positive and negative particles respectively[9],

$$\mu_\pm^{\text{chem}} = k_\text{B}T \log\left(\frac{c_\pm}{c_0}\right) + \mu_{0,\pm} \tag{2.20}$$

where k_B is the Boltzmann constant, T is the temperature, c_0 is a chosen reference concentration and $\mu_{0,\pm}$ is the chemical potential for a positively/negatively charged particle in a solution of concentration c_0.

Another contribution to the electrochemical potential is from the electric potential. A particle of charge $\pm|Z|e$ gains the energy $\pm|Z|e\phi$ in the presence of an electric potential ϕ. Thus we write the full electrochemical potential as

$$\mu_\pm = k_\text{B}T \log\left(\frac{c_\pm}{c_0}\right) \pm |Z|e\phi + \mu_{0,\pm}. \tag{2.21}$$

As mentioned in the introduction we have omitted the dependencies. We emphasize though, that both $c_\pm$, ϕ and thus $\mu_\pm$ is a function of $\boldsymbol{r}$ while μ_0 is a constant. The electrochemical potential together with advection governs the flow of particles in a solution,

$$\boldsymbol{J}_\pm = c_\pm \boldsymbol{v} - c_\pm \frac{D_\pm}{k_\text{B}T}\boldsymbol{\nabla}\mu. \tag{2.22}$$

Neglecting advection, particles (and/or heat) will flow from areas with high electrochemical potential to low until the system reaches thermodynamic equilibrium,

$$\boldsymbol{\nabla}\mu = 0 \quad \text{(thermodynamic equilibrium)}. \tag{2.23}$$

3 | Electrolyte near charged wall

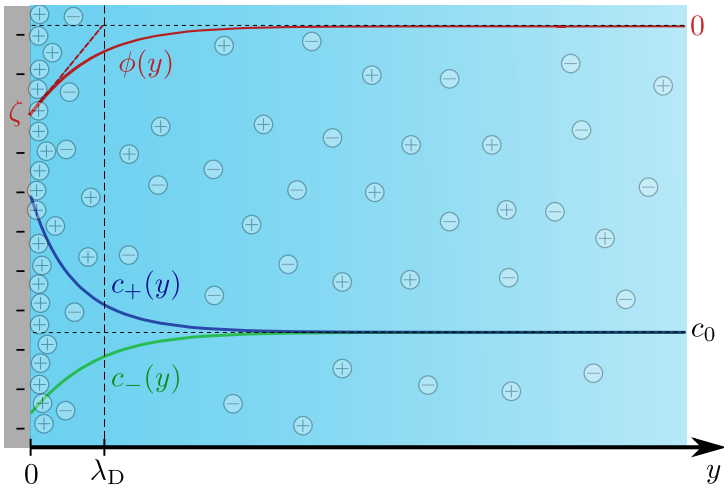

Figure 3.1: Sketch of an electrolyte with cations and anions near a negatively charged wall. $\phi(y)$ shows the electric potential, $c_+(y)$ (blue) and $c_-(y)$ (green) show the cation and anion concentration respectively which both approache c_0 far from the wall. The Debye length λ_D is marked with a vertical line.

In this chapter we will investigate how the electric potential and the ionic concentrations behave near a charged wall. We consider a infinite plane wall in the zx plane as shown in Fig. 3.1. Practically the wall could be made of silica which by chemical interaction with water at the surface give rise to a charge displacement leaving the wall more negative and the electrolyte more positive[2].

3.1 The ionic concentrations

In thermodynamic equilibrium the chemical potential is constant throughout the entire system,

$$\boldsymbol{\nabla}\mu_\pm = k_B T \boldsymbol{\nabla} \ln\left(\frac{c_\pm(\boldsymbol{r})}{c_0}\right) \pm |Z| e \boldsymbol{\nabla}\phi(\boldsymbol{r}) = 0. \tag{3.1}$$

Now, we assume that both positive and negative ions approach the same concentration $c\pm(\infty) = c_0$ infinitely far away from the wall and that the potential goes to zero, $\phi(\infty) = 0$. With these boundary conditions, Eq. (3.1) is easily integrated and solved for $c_\pm$,

$$c_\pm(\boldsymbol{r}) = c_0 \ \exp\left(\mp\tilde{\phi}(\boldsymbol{r})\right). \tag{3.2}$$

where we have introduced the normalized $\tilde{\phi} = \phi/V_\mathrm{T}$. Not surprisingly, since we have used the ideal gas approximation, the concentration of ions is proportional to the Boltzmann factor. Analytical and numerical solutions for Eq. (3.2) are plotted near the wall in Fig. 3.2(a), using the Gouy-Chapmann potential derived in the following. We notice that the cation concentration increases more than the anion concentration decreases so that a net charge density is formed near the wall.

3.2 The electric potential

Defining the charge density $\rho_\mathrm{el} \equiv |Z|e(c_+^\mathrm{i} - c_-)$, we combine the Poisson equation Eq. (2.14b) and the Boltzmann distribution of ions Eq. (3.2) to arrive at the Poisson-Boltzmann equation,

$$\nabla^2\tilde{\phi}(\boldsymbol{r}) = \frac{1}{\lambda_\mathrm{D}^2}\sinh\left(\tilde{\phi}(\boldsymbol{r})\right), \tag{3.3}$$

where we have introduced the Debye length,

$$\lambda_\mathrm{D} \equiv \sqrt{\frac{\epsilon V_\mathrm{T}}{2|Z|ec_0}}. \tag{3.4}$$

Note that ϵ is the permittivity of the electrolyte, which we assume is the same as for pure water $\epsilon_\mathrm{w} = 80.1\,\epsilon_0$[6].

Eq. (3.3) is really cumbersome to solve and in most cases impossible so that only numerical solutions are available. However for the one dimensional case shown in Fig. 3.1 the Gouy-Chapman solution applies[5]. In dimensionless form it reads,

$$\tilde{\phi}(y) = 4\tanh^{-1}\left[\tanh\left(\tilde{\zeta}/4\right)\exp\left(-y/\lambda_\mathrm{D}\right)\right] \quad \text{for} \quad \phi(\boldsymbol{r}) = \phi(y), \tag{3.5}$$

satisfying $\tilde{\phi}(\infty) = 0$ and $\tilde{\phi}(0) = \tilde{\zeta}$. Here we have defined the normalized zeta-potential $\tilde{\zeta}$ as the potential at the wall, $\tilde{\zeta} \equiv \zeta/V_\mathrm{T} = \phi(0)/V_\mathrm{T}$. In some cases it might be more convenient to work with the surface charge σ on the wall instead of the the zeta potential. Therefore we search for a relation between the surface charge and the zeta potential. The gradient of the potential at the wall is easily found by integrating Eq. (3.5) once[2]

$$\partial_y\tilde{\phi}(0) = -\frac{1}{\lambda_\mathrm{D}}2\sinh\left(\tilde{\zeta}/2\right), \tag{3.6}$$

satisfying the boundary conditions $\tilde{\phi}(\infty) = \partial_y\tilde{\phi}(\infty) = 0$ and $\partial_y\tilde{\phi} > 0$ for $y > 0$. We consider the wall and the electrolyte as a capacitor and apply the standard condition that

the electric field outside the capacitor is vanishing[10]. Thus by the well known Gaussian box argument we find that $\sigma = \epsilon_{\mathrm{w}} E(0) = \epsilon_{\mathrm{w}}(-\partial_y \phi(0))$ which by Eq. (3.6) yields,

$$\sigma = \frac{2V_{\mathrm{T}}\epsilon_{\mathrm{w}}}{\lambda_{\mathrm{D}}} \sinh\left(\tilde{\zeta}/2\right), \tag{3.7}$$

which is the relation between the ζ and σ we searched for.

The equations simplifies a lot in the important case of low potentials, also known as the Debye-Hückel limit, i.e. when $|Z|e\zeta \ll k_B T$. In this case Eq. (3.3) can be linearized as

$$\nabla^2 \phi(\boldsymbol{r}) = \frac{1}{\lambda_{\mathrm{D}}^2}\phi(\boldsymbol{r}) \quad \text{for} \quad |Z|e\zeta \ll k_{\mathrm{B}}T. \tag{3.8}$$

From this equation the potential is easily found for the one dimensional case,

$$\phi(y) = \zeta \exp\left(-\frac{y}{\lambda_{\mathrm{D}}}\right) \quad \text{for} \quad |Z|e\zeta \ll k_{\mathrm{B}}T, \tag{3.9}$$

satisfying the same boundary conditions, $\phi(0) = \zeta$ and $\phi(\infty) = 0$. In this equation the Debye length is easily interpreted as the characteristic length scale with which the potential decreases.

As sketched in Fig. 3.1 the exponential solution to the potential has the property $\partial_y \phi(0) = -\phi(0)/\lambda_{\mathrm{D}} = -\zeta/\lambda_{\mathrm{D}}$, so that Eq. (3.7) simplifies to

$$\sigma = \frac{\epsilon_{\mathrm{w}}}{\lambda_{\mathrm{D}}}\zeta \quad \text{for} \quad |Z|e\zeta \ll k_{\mathrm{B}}T, \tag{3.10}$$

which is also obtained directly by linearising Eq. (3.7). The Debye-Hückel and the Gouy-Chapman potential have been plotted together with numerical solutions in Fig. 3.2(b) near the membrane for different wall charges. Both the Gouy-Chapmann and the Debye-Hückel potential are seen to be in good agreement with numerical solutions for small wall charge whereas only the Gouy-Chapman potential follow the numerical solutions for more negative wall charges.

3.2.1 The Debye Length

In the case of a charged wall, the Debye length gives the thickness of the screening layer on the wall. We shall assume relatively weak concentrations of around 1 mM, so that the Debye length is around 10 nm at room temperature. Note that this length scale is in the order of the fluid particle introduced in the introduction and thus we should be aware when interpreting results involving this screening layer.

3.2.2 The Debye-Hückel limit

The Debye-Hückel solution is simple and easy to use for a lot of problems. But if we choose a wall charge of around $1\,\mathrm{mC\,m^{-2}}$ and a Debye length of around 10 nm, we get zeta potential 14 meV, which is close the thermal energy at room temperature, $k_{\mathrm{B}}T \approx 26$ meV

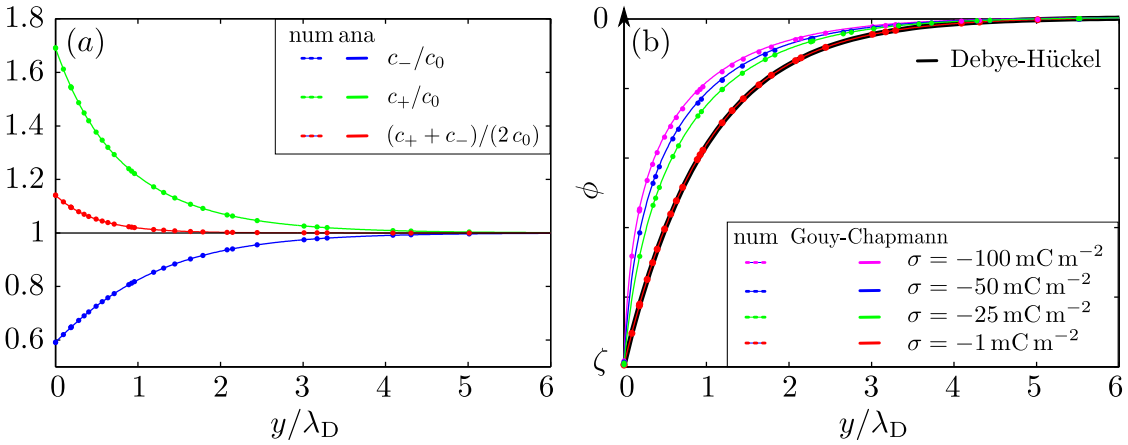

Figure 3.2: (a) Analytical and numerical solutions for cation and anion concentrations normalised to c_0 for $\sigma = -1$ mC/m^2. Analytical solutions are plotted for Eq. (3.2), using the Gouy-Chapmann potential Eq. (3.5). (b) Decaying electric potentials for three different wall charges plotted together with the Debye-Hückel approximation. Numerical setup is described in Chapter 5.

so that the Debye-Hückel approximation will be on the limit to break down. The Gouy-Chapman solution on the other hand is always valid for one dimensional problems as shown in Fig. 3.2. It only suffers from the fact that it only works for single walls. However imagine that two parallel plates lies sufficiently far away from each so that the potential from each wall has fallen to a vanishing level at the center. Then we can treat each plate as a single plate and thus apply the Gouy-Chapman potential.

4 | Numerical modeling

In this chapter we present The Finite Element Method (FEM) and how to implement it in the software COMSOL MULTIPHYSICS. This chapter will introduce the general deductions of the theory needed for further analysing in later chapters.

4.1 The Finite Element Method

Solving the Navier-Stokes equation analytically can be a complex and sometimes impossible problem. FEM is a method for both solving ordinary and partial differential equations and is used in a vast varieties of problems within science and engineering. Among these problems comes fluid dynamics. The core idea of FEM is to to split the domain of interest into many small sub domains and thereby solving each sub domain independently. Each domain in FEM is called a grid. The geometric form of the grid varies from problem to problem. For each grid a node is associated to each corner of the grid. Each grid is associated with some basis functions which values runs from 1 on the node to 0 on the neighbour node. The basis functions can be chosen as desired but often polynomials are chosen as the are easy for a computer to both differentiate and integrate. The order of the polynomial often depend of how the function of interest varies on the specific region.

Our general problem is to solve an inhomogeneous PDE. We start by looking at a general partial differential equations with a boundary term

$$\mathcal{L}\{g(\boldsymbol{x})\} = F(\boldsymbol{x}), \tag{4.1}$$

where $\mathcal{L}$ denotes a differential operator working on our function $g(\boldsymbol{x})$, and $F(\boldsymbol{x})$ is some source term. An equation which satisfy Eq. (4.1) is called a strong solution. But in the case where we need to use approximate solutions this equation can no longer be satisfied and we therefore need to introduce the so-called deffect defined as

$$d(\boldsymbol{x}) \equiv \mathcal{L}\{g(\boldsymbol{x})\} - F(\boldsymbol{x}). \tag{4.2}$$

If the defect equals zero we simply have Eq. (4.1) again. To get an approximate solution for the function g we expand it in terms of some finite basis functions

$$g(\boldsymbol{x}) = \sum_n c_n \psi_n. \tag{4.3}$$

where c_n are the expansion coefficients. At the n'th node ψ_n takes the value 1 and therefore c_n takes the value of $g(\boldsymbol{x})$ at the n'th node.

In order to find the best solution for Eq. (4.1) we demand the inner product between the expansion coefficients and the defect to vanish

$$\langle \psi_m, d(\boldsymbol{x}) \rangle = 0, \quad \text{for all } m. \tag{4.4}$$

We define the inner product between two real functions as $\langle a(\boldsymbol{x}), b(\boldsymbol{x}) \rangle \equiv \int_\Omega a(\boldsymbol{x}) b(\boldsymbol{x})\, d\boldsymbol{x}$. Next step is to substitute the defect into Eq. (4.4). In the case where the operator $\mathcal{L}$ is linear (in this report we shall use the linear differential operator) the sum and expansion coefficients can be taken outside the integral and we arrive at the following equation[11],

$$\sum_n c_n \langle \psi_m, \mathcal{L}\psi_n \rangle = \langle \psi_m, F(\boldsymbol{x}) \rangle, \quad \text{for all } m. \tag{4.5}$$

We recognize that the left hand side can be written as a matrix-vector product and the right hand side as a vector. This leads to the following matrix-vector product

$$\boldsymbol{K}\boldsymbol{a} = \boldsymbol{F}(\boldsymbol{x}), \tag{4.6}$$

where $\boldsymbol{K}$ is called the stiffness matrix. Solving this matrix equation for the coefficients c_n exactly yields the weak solution which is exactly what we wanted. As the number of basis functions in Eq. (4.3) is only finite the weak formulation will only be approximately. To obtain a strong solution one would require the span of basis function to go to infinity.

4.1.1 The weak formulation

One of the most crucial parts of solving the boundary value problems by FEM is the implementation of boundary condition. Two different kind of boundary conditions will be introduced, namely the Dirichlet and the Neumann conditions which uses the function value and the flux at the giving boundary respectively. We consider a continuity equation of the form of Eq. (4.1)

$$\boldsymbol{\nabla} \cdot \boldsymbol{\Gamma} = \boldsymbol{F}(\boldsymbol{x}). \tag{4.7}$$

Solving the continuity equations in this way is interesting since we can write all the governing equations used in this thesis in this form. Now, inserting Eq. (4.13) into Eq. (4.2) we have

$$\langle \psi_m, \boldsymbol{\nabla} \cdot \boldsymbol{\Gamma} - \boldsymbol{F}(\boldsymbol{x}) \rangle = \int_\Omega \psi_m \boldsymbol{\nabla} \cdot \boldsymbol{\Gamma} - \psi_m\, \boldsymbol{F}(\boldsymbol{x})\, d\boldsymbol{x} = 0. \tag{4.8}$$

Using the product rule for integration, we rewrite Eq. (4.8) to

$$\int_\Omega \boldsymbol{\nabla} \cdot (\psi_m \boldsymbol{\Gamma}) - (\boldsymbol{\nabla}\psi_m) \cdot \boldsymbol{\Gamma} - \psi_m\, \boldsymbol{F}(\boldsymbol{x})\, d\boldsymbol{x} = 0. \tag{4.9}$$

Now the first integrand of Eq. (4.9) can by Gauss' divergence theorem be written as an integral over the boundary and we finally get

$$\int_{\delta\Omega} \psi_m\, \boldsymbol{n} \cdot \boldsymbol{\Gamma}\, d\boldsymbol{x} + \int_\Omega - (\boldsymbol{\nabla}\psi_m) \cdot \boldsymbol{\Gamma} - \psi_m\, \boldsymbol{F}(\boldsymbol{x})\, d\boldsymbol{x} = 0. \tag{4.10}$$

The boundary conditions

The Neumann boundary conditions are used in the case of a known flux through the specific area. Defining the flux as a function $h(\boldsymbol{x})$ we can make the following substitution in Eq. (4.10)

$$h(\boldsymbol{x}) = \boldsymbol{n} \cdot \boldsymbol{\Gamma} \text{ for } \boldsymbol{x} \in \partial\Omega. \tag{4.11}$$

In the Dirichlet boundary a constraint is introduced on the boundary. That is, we now know the value of the function on the boundary

$$j(\boldsymbol{x}) = g(\boldsymbol{x}) \text{ for } \boldsymbol{x} \in \partial\Omega. \tag{4.12}$$

To implement the constraint in the weak form, the Lagrange multiplier $\lambda(\boldsymbol{r})$ is introduced. The multiplier consist of a new list of basis functions, which are all required to be orthogonal to the constraint. As required in Eq. (4.12) the constraint only lives on the boundary. Adding the product of the constraint Eq. (4.12) and the Lagrange multiplier to Eq. (4.13) gives the continuity equations modified with the desired constraint

$$\boldsymbol{\nabla} \cdot \boldsymbol{\Gamma} = \boldsymbol{F}(\boldsymbol{x}) + \sum_n \lambda(\boldsymbol{r}) \hat{g}_n(\boldsymbol{r}), \tag{4.13}$$

where the n'th $\lambda(\boldsymbol{r})$ is changed to satisfy the constraints[12, 13].

4.1.2 Mesh Convergence

The test functions mentioned above take the value one on the nodes. These nodes form elements which together form what we call a mesh. The sizes of the mesh have a huge impact on the quality of the solutions. Too big meshes will result in misleading solutions where the solutions depend on the mesh size rather than the real physics. On the other hand too small meshes demand more computational power.

The size of the mesh depends highly on how the function of interest varies locally. In the channels of micrometre scale an extremely small mesh is needed close to the wall where the scale is dominated by the Debye length. Later on a model in millimetre scale is presented where nanometre size mesh is impossible with the computers available and approximations in our models to allow for bigger mesh is crucial for the computational time.

We see from figure Fig. 4.1 (b) how the maximum mesh size is much smaller at the boundaries than in the bulk. The bottom line is a symmetry line and because require no stricter mesh size than the rest of the bulk. The mesh is made of nodes connected to each other in triangles but could also be made up of other kind of geometric structures. This can be changed in Comsol and different geometries are advantageous in different problems but the choice of geometry have not been investigated and triangles have then been chosen because of its general validity.

In order to find an appropriated mesh size we will now present a method to evaluate the mesh quality. We will define the value of a dependent variable of finest mesh possible

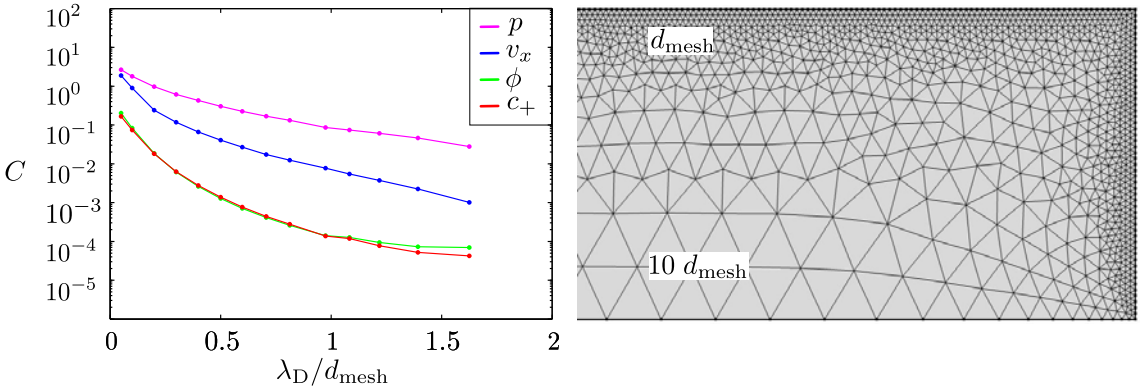

Figure 4.1: (a) Mesh convergence analysis showing a semi-logarithmic plot of the relative mesh convergence parameter for the dependent variables ϕ, c_+, v_x, and p for different λ/d_{mesh} and $\sigma = -1\text{mC/m}^2$ and $V_0 = 5V_{\text{T}}$, and (b) The mesh visualised in upper right corner of a channel modeled in Chapter 5. The mesh has a size of maximum d_{mesh} at the boundaries and maximum 10 d_{mesh} in the bulk.

by g_{ref} which will work as a reference. A given value for a dependent value for a coarser mesh is denoted g, and we define the relative convergence parameter as [14]

$$C(g) = \sqrt{\frac{\int_\Omega \mathrm{d}A\ (g - g_{ref})^2}{\int_\Omega \mathrm{d}A\ (g_{ref})^2}}. \tag{4.14}$$

We will define the finest mesh size with $d_{\text{mesh}} = \lambda_D/2$, where λ_D is the Debye length, set to $\lambda_D = 9.7$ nm. Now varying d_{mesh} we can calculate Eq. (4.14) for different mesh sizes. On the boundaries we require a the biggest to be d_{mesh} and in the bulk the mesh must not exceed $10d_{\text{mesh}}$.
Fig. 4.1 plots Eq. (4.14) for the dependent variables ϕ, c_+, v_x, and p. The different fields converges considerably faster for d_{mesh} bigger than the Debye length followed by a much slower convergence. This behaviour is not surprisingly since the equilibrium potential varies with the Debye length and we therefore expect to use a mesh resolution in the order of the Debye length. To ensure that we can rely on numerical solution from Comsol we require d_{mesh} never to be greater than the Debye length.

5 | Microchannel

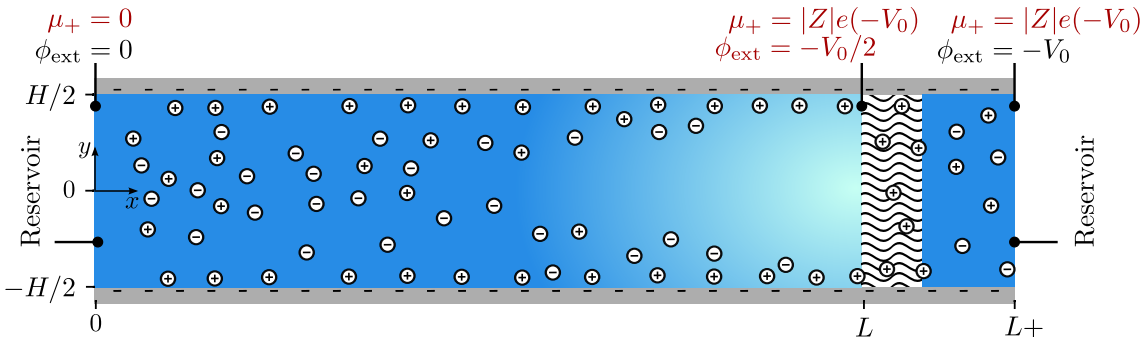

Figure 5.1: Sketch of a microchannel of length L and height H with a cation selective membrane at $x = L$. Both H and L are in the order of μm. At the walls we have negative surface charge and in the bulk we have both cations and anions. At $x = 0$ and after the membrane at $x = L+$ we have reservoirs with $c_\pm = c_0$. Electrodes on each side of the membrane at $x = 0$ and $x = L+$ establishes an electric potential drop of $-V_0$ across the the channel (black text at top). The red text at the top denotes physical consequences from this setup. Note that from $x = 0$ to $x = L$ the potential drop is only $V_0/2$.

The scope of this thesis is to understand electrokinetic behavior in microsystems in detail and then use this knowledge to suggest a model for ion separation on a larger scale. In Chapters 6 and 7 we shall work with porous medium to effectively form a network of micro channels. In this chapter we present an investigation of a single idealised microchannel as shown in Fig. 5.1.
We start by presenting the physical setup of our microchannel. Next we make some analytical models on how potentials, concentrations and flow behave. Finally we present our numerical setup in COMSOL. Analytical results will throughout the chapter be compared with numerical simulations. Depletion and charge polarization will be of the important keywords in the interpretations of the results.

5.1 Physical setup

We will be analysing porous media made of silica which tend to have a negative surface charge due to chemical reactions with water[2]. For this reason we will consider a mi-

crochannel with negative walls. In each end of the channel a reservoir with a common cation and anion concentration $c_\pm = c_0$ is situated. One could imagine a reservoir being a steady flow securing a constant concentration. At $x = L$ we place a cation selective membrane which could be a nafion membrane, which is a medium with a fixed negative surface charge so that anions are excluded and cations are let through with high conductivity. The nafion membrane has very narrow hydrophilic pores with size in the order of angstroms[15] so for the flow we model the membrane as a normal wall with no slip boundary condition. We apply an external electric field over the channel by setting electrodes at $x = 0$ and $x = L+$ (see Fig. 5.1). Since the concentration at the electrodes is $c_\pm = c_0$ this leads to an electrochemical potential difference of ZeV_0 over the channel as indicated with red text at the top of Fig. 5.1.

5.2 The electrochemical potential through the channel

We can split the total electric potential into two parts. ϕ_{ext} which is the external potential that we establish with the electrodes, and ϕ_{eq} which is an equilibrium potential that we defined in Chapter 3. Thus we write the total electric potential as

$$\phi_{\text{tot}}(x, y) \equiv \phi_{\text{eq}}(x, y) + \phi_{\text{ext}}(x). \tag{5.1}$$

Please note that ϕ_{eq} depends on both x and y since concentration variation through the channel changes the Debye ength. ϕ_{ext} on the other hand is only a function of x.

As usually we use the Boltzmann distribution to describe how the ion concentrations dependent on the electric potential when in thermodynamic equilibrium with respect to the vertical direction,

$$c_\pm(x, y) = c(x)\ \exp(\mp\tilde{\phi}_{\text{eq}}(x, y)), \tag{5.2}$$

where $c(x)$ is the common concentration for c_+ and c_- in the limit infinitely far away from the wall. If the concentration changes through the channel due to the external potential this is not necessarily c_0. We can find $c(x)$ by using that the anions distribute in the horizontal direction such as to establish thermodynamic equilibrium. In dimensionless form with $\tilde{\mu} = \mu/(k_{\text{B}}T)$ and $\tilde{c} = c/c_0$ we then have

$$\partial_x\tilde{\mu}_- = \partial_x\left(\log(\tilde{c}_-) - \tilde{\phi}_{\text{tot}}\right) \tag{5.3a}$$

$$= \partial_x\left(\log(\tilde{c}) + \tilde{\phi}_{\text{eq}} - (\tilde{\phi}_{\text{eq}} + \tilde{\phi}_{\text{ext}})\right) \tag{5.3b}$$

$$= \partial_x\left(\log(\tilde{c}) - \tilde{\phi}_{\text{ext}}\right) = 0, \tag{5.3c}$$

which is easily integrated so that

$$c(x) = c_0 \exp(\tilde{\phi}_{\text{ext}}(x)), \tag{5.4}$$

satisfying $c(0) = c_0$. With this value we see that,

$$\tilde{\mu}_+ = \log(\tilde{c}_+) + \tilde{\phi}_{\text{tot}} \tag{5.5a}$$

$$= \log\left(c \exp(-\tilde{\phi}_{\text{eq}})\right) + (\tilde{\phi}_{\text{eq}} + \tilde{\phi}_{\text{ext}}) \tag{5.5b}$$

$$= \tilde{\phi}_{\text{ext}} - \tilde{\phi}_{\text{eq}} + (\tilde{\phi}_{\text{eq}} + \tilde{\phi}_{\text{ext}}) = 2\,\tilde{\phi}_{\text{ext}}. \tag{5.5c}$$

Note that this equation is only valid where the anions are in horizontal thermodynamic equilibrium i.e. from $x = 0$ to $x = L$.

5.3 The electric potential at the membrane

Using Eq. (5.5) and the fact that $c_+(L+) = c_0$ at the right reservoir, we can write the chemical potential for cations at membrane and after the membrane respectively,

$$\tilde{\mu}_+(L) = 2\tilde{\phi}_{\text{ext}}(L) \tag{5.6a}$$

$$\tilde{\mu}_+(L+) = -\tilde{V}_0. \tag{5.6b}$$

We can argue that these two equations are equal by the folowing considerations:
In a very short time after applying an external electric field over the microchannel, the anions will distribute such as to reach thermodynamic equilibrium as mentioned. The cations on the other hand which are allowed to pass through the membrane will contribute to a steady current governed by the gradient of the electrochemical potential from Eq. (2.22),

$$J_+ = -\frac{D_+}{k_{\text{B}}T} c_+^{\text{i}} \partial_x \mu_+. \tag{5.7}$$

To write this equation we have made two assumptions. Firstly we have assumed the channel to be long and symmetric so that there is no current in the y-direction and the problem reduces to one dimension. Secondly we have assumed that advective current is negligible compared to electrophoretic current. This is a good approximations for channel heights much larger than the Debye length[5] which is satisfied in this model with a height of $1\,\mu$m and a Debye length of 10 nm.
If we assume no chemical reactions, it can be seen from Eq. (2.15b) that a one dimensional current density will be constant through the channel and through the membrane. Thus inside the membrane, where we have a high concentration of cations c_+^{i}, we find that the chemical potential must be almost constant over the membrane to keep J_+ fixed. Thus we can find the electric potential at the membrane by equating Eq. (5.6a) with Eq. (5.6b),

$$\mu_+(L) = \mu_+(L+) \Rightarrow \phi_{\text{ext}}(L) = -\frac{V_0}{2}, \tag{5.8}$$

so that half of the external electric potential drop lies over the membrane alone.

We will in the following treat the microchannel in the two cases with and without wall charges.

5.4 Uncharged walls

In the following we shall assume charge neutrality so that $c_+^{\mathrm{i}} = c_- = c_0 \exp\tilde{\phi}_{\mathrm{ext}}$ for no wall charge, so that $\tilde{\phi}_{\mathrm{eq}} = 0$. The assumption of charge neutrality is discussed in Section 5.4.1. Inserting Eq. (5.5) into Eq. (5.7), the cation current density is easily found,

$$J_+ = -D_+ c_+^{\mathrm{i}} \partial_x \tilde{\mu}_+ \tag{5.9a}$$

$$= -D_+ \left(c_0 \exp(\tilde{\phi}_{\mathrm{ext}}) \right) \partial_x (2\,\tilde{\phi}_{\mathrm{ext}}) \tag{5.9b}$$

$$= -(2D_+ c_0/L)\, \partial_{\tilde{x}} \exp(\tilde{\phi}_{\mathrm{ext}}), \tag{5.9c}$$

where we in the last step changed to the dimensionless $\tilde{x} \equiv xL^{-1}$. We normalize by the prefactor $(2D_+c_0/L)$,

$$\tilde{J}_+ \equiv \frac{J_+}{2D_+c_0/L} = \partial_{\tilde{x}} \exp(\tilde{\phi}_{\mathrm{ext}}). \tag{5.10}$$

This is easily integrated since J_+ is a constant throughout the channel,

$$\tilde{J}_+ \tilde{x} = 1 - \exp(\tilde{\phi}_{\mathrm{ext}}) \tag{5.11a}$$

$$\tilde{J}_+ = 1 - \exp(-\tilde{V}_0/2), \tag{5.11b}$$

satisfying $\tilde{\phi}_{\mathrm{ext}}(0) = 0$ and $\tilde{\phi}_{\mathrm{ext}}(1) = -\tilde{V}_0/2$. From Eq. (5.11b) we see that the maximum current of cations for uncharged walls is exactly $2D_+c_0/L$, which is known in the literature as the limiting current[3]. We see from Fig. 5.3(a) that the cation current density for no wall charge ($\sigma = 0$) agrees with numerical solutions. From Eqs. (5.11a) and (5.11b) we find an expression of the external potential,

$$\tilde{\phi}_{\mathrm{ext}}(\tilde{x}) = \ln\left[1 - \tilde{J}_+\tilde{x}\right] = \ln\left[1 - \left(1 - \exp(-\tilde{V}_0/2)\right)\tilde{x}\right]. \tag{5.12}$$

And hence we can find the ionic density,

$$c_+ = c_0 \exp(\tilde{\phi}_{\mathrm{ext}}) = c_0\left[1 - \left(1 - \exp(-\tilde{V}_0/2)\right)\tilde{x}\right]. \tag{5.13}$$

From Eq. (5.13) we expect that the concentration is linear through the channel so that no depletion region occurs. However as we show in Fig. 5.4(b) ($\sigma = 0$), we find that the numerical solutions gives a depletion region for potentials higher than $\tilde{V}_0 = 10$. This is due to the fact, that the assumption of charge neutrality breaks down for higher potentials. We also see that the potential found in Eq. (5.12) certainly does not satisfy the one dimensional Laplace equation, $\partial_{\tilde{x}}^2 \tilde{\phi}_{\mathrm{ext}} = 0$. We discuss break down of charge neutrality in the following section.

5.4.1 Break down of charge neutrality

One argument for charge neutrality is seen by considering the one dimensional normalised Poisson equation,

$$\partial_{\tilde{x}}^2 \tilde{\phi}_{\mathrm{ext}} = -\frac{L^2}{2\lambda_{\mathrm{D}}^2}(\tilde{c}_+ - \tilde{c}_-). \tag{5.14}$$

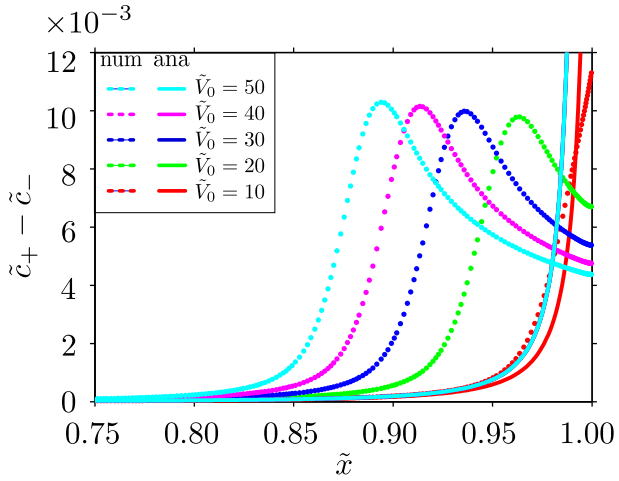

Figure 5.2: Numerical solutions of the ionic concentration differences normalised to the reservoir concentration c_0, plotted versus $\tilde{x} = xL^{-1}$ for the last 25 percent of the channel. The solutions are compared with the analytic result from Eq. (5.15). Note that all analytic lines above $\tilde{V}_0 = 10$ overlaps.

We see that since $\lambda_D \ll L$, a small difference in the ionic concentrations leads to a huge change in the electric field acting to equalise the difference. However if we insert Eq. (5.12) into Eq. (5.14), we find that

$$\tilde{c}_+ - \tilde{c}_- = \frac{2\lambda_D^2}{L^2} \frac{\tilde{J}_+^2}{(1 - \tilde{J}_+ \tilde{x})^2} \tag{5.15}$$

so that the charge neutrality breaks down near the membrane for high external potentials. This point is illustrated in Fig. 5.2 where numerical simulations of $\tilde{c}_+ - \tilde{c}_-$ has been made for different potentials and compared with the result from Eq. (5.15). In agreement with Eq. (5.15) the numerical solutions give a charge polarization in front of the membrane. However as seen in the Fig. 5.2 the analytical results only cache the beginning of this behavior. In the numerical solution we see that the charge density reaches a maximum before the membrane. This can be understood as an effect from the strong external electric field near the membrane accelerating the cations so that the concentration is lowered to keep a constant current density.

5.5 Charged walls

We now consider a channel with wall charge σ. We will in this section see how a cation current density along the walls leads to an overlimiting current and an extended depletion region in front of the membrane.
For the case with $\sigma = 0$ we had concentration gradient in the y-direction. Now with $\sigma < 0$ the behavior described in Chapter 3 applies and we will expect a higher concentration of

cations near the wall screening the negative wall charge. Thus we do not expect complete charge neutrality in the bulk but we expect that the sum of all charges in the bulk *and* on the walls is zero,

$$|Z|eH\left(\langle c_+\rangle - \langle c_-\rangle\right) + 2\sigma = 0, \tag{5.16}$$

where $\langle\cdot\rangle$ denotes averaging across the channel from $-H/2$ to $H/2$. We see that for negative wall charge we have a higher concentration of cation in the bulk in order to maintain total charge-neutrality. This high concentration of cations will mainly be near the negative walls as shown in Chapter 3. We will now derive an expression for the cation current in the same way as we did for the case with no wall charge. Normalising Eq. (5.16),

$$\langle \tilde{c}_+\rangle = \langle \tilde{c}_-\rangle - \tilde{\rho}_\mathrm{s} \approx \exp(\tilde{\phi}_\mathrm{ext}) - \tilde{\rho}_\mathrm{s}, \tag{5.17}$$

where the normalised averaged wall charge is defined as,

$$\tilde{\rho}_s \equiv \frac{2\sigma}{|Z|eHc_o}. \tag{5.18}$$

Note that in Eq. (5.17) we have assumed that the average anion concentration over a vertical cross section is just the same as for no wall charge. This can be considered in two limits: For low ζ-potentials c_- only varies a little near the wall so that for a wide channel the average concentration is approximately c_0. For high ζ-potentials c_+^i is very high near the wall, but c_- is limited by $0 \leq \frac{c_-}{c_0} \leq 1$ and as the zeta potential gets higher the anions are only depleted in a very small area in front of the wall so that the average concentration of anions over the hole channel is still approximately c_0.

Similar to before we now find the averaged cation current by combining Eqs. (5.5) and (5.7),

$$\begin{aligned} 2\langle \tilde{J}_+\rangle &= \langle -\tilde{c}_+\partial_{\tilde{x}}\tilde{\mu}_+\rangle && \text{(5.19a)}\\ &= \langle -\tilde{c}_+\partial_{\tilde{x}}(2\,\tilde{\phi}_\mathrm{ext})\rangle && \text{(5.19b)}\\ &= \langle -\tilde{c}_+\rangle\partial_{\tilde{x}}(2\,\tilde{\phi}_\mathrm{ext}). && \text{(5.19c)} \end{aligned}$$

In the last step we have used that ϕ_ext is constant in y. Inserting Eq. (5.17) yields

$$\begin{aligned} \langle \tilde{J}_+\rangle &= -\left(\exp(\tilde{\phi}_\mathrm{ext}) - \tilde{\rho}_\mathrm{s}\right)\partial_{\tilde{x}}\tilde{\phi}_\mathrm{ext} && \text{(5.20a)}\\ &= -\partial_{\tilde{x}}\left(\exp(\tilde{\phi}_\mathrm{ext})\right) + \tilde{\rho}_\mathrm{s}\partial_{\tilde{x}}\tilde{\phi}_\mathrm{ext}. && \text{(5.20b)} \end{aligned}$$

Again $\langle \tilde{J}_+\rangle$ is constant throughout the channel and Eq. (5.20b) is easily integrated,

$$\begin{aligned} \langle \tilde{J}_+\rangle\tilde{x} &= 1 - \exp(\tilde{\phi}_\mathrm{ext}) + \tilde{\rho}_\mathrm{s}\tilde{\phi}_\mathrm{ext} && \text{(5.21a)}\\ \langle \tilde{J}_+\rangle &= 1 - \exp(-\tilde{V}_0/2) - \tilde{\rho}_\mathrm{s}(\tilde{V}_0/2) && \text{(5.21b)} \end{aligned}$$

satisfying $\tilde{\phi}_\mathrm{ext}(0) = 0$ and $\tilde{\phi}_\mathrm{ext}(1) = -\frac{V_0}{2}$ as usual. We notice that for no wall charge $\tilde{\rho}_s = 0$, and Eq. (5.21b) reduces to Eq. (5.11b).
For small potentials the term $-\exp(-\tilde{V}_0/2)$ in Eq. (5.21b) dominates. For increasing

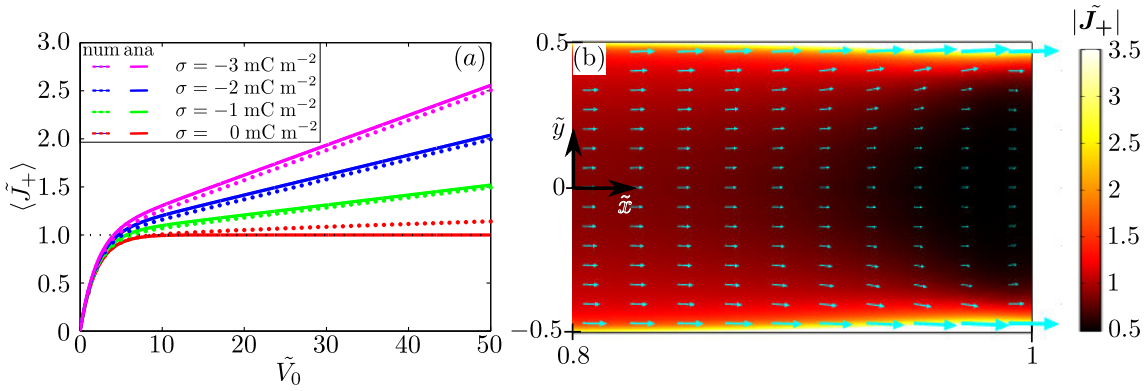

Figure 5.3: (a) The cation current density $\langle \tilde{J}_+ \rangle$ averaged over a vertical cross section plotted versus the potential $\tilde{V}_0$ for different wall charges. (b) 2D plot of the cation current for $\tilde{V}_0 = 10$. Arrows indicate the vector field (proportional) and colors indicate the scalar field $|\tilde{\boldsymbol{J}}_+|$.

potentials this term approach zero and the so-called limiting current is reached. Now, due to the wall charges, a high concentration of cations are located near the wall and a current of positive ions is allowed in this region. This gives rise to the so-called overlimiting current[3]. In Fig. 5.3(a) we plot Eq. (5.21b) for different wall charges. Numerical solutions are seen to be in good agreement except for $\sigma = 0$ mC m^{-2}. In this case we see a small overlimiting current due charge polarisation near the membrane as described in Section 5.4.1.

We write the analytical expression for the external potential by solving Eq. (5.21a)[16],

$$\tilde{\phi}_{\text{ext}} = -W\left(-\frac{\exp\left((\tilde{J}_+\tilde{x}-1)/\tilde{\rho}_s\right)}{\tilde{\rho}_s}\right) + \frac{(\tilde{J}_+\tilde{x}-1)}{\tilde{\rho}_s}, \tag{5.22}$$

where $W(z)$ is the Lambert W function satisfying $z = W(z)\exp(W(z))$. In Fig. 5.5 Eq. (5.22) is plotted versus numerical solutions. As expected an external potential drop of $\tilde{V}_0/2$ is seen. We can now find $\langle c_+^{\text{i}} \rangle$ by inserting Eq. (5.22) into Eq. (5.17). $\langle c_+^{\text{i}} \rangle$ is plotted in Fig. 5.4(a) where we see an extended depletion region for higher surface charges. Please notice that $\langle c_+^{\text{i}} \rangle$ never goes to zero due to the cations in the Debye layer. We can also isolate x by combining Eqs. (5.17) and (5.21)

$$\tilde{x} = \frac{1 - (\langle \tilde{c}_+ \rangle + \tilde{\rho}_s) + \tilde{\rho}_s \log\left(\langle \tilde{c}_+ \rangle + \tilde{\rho}_s\right)}{1 - \exp(-\tilde{V}_0/2) - \tilde{\rho}_s(\tilde{V}_0/2)}. \tag{5.23}$$

Please notice that from this equation the size of the depletion region relative to the length of the channel, $1-\tilde{x}$, is constant for a given potential. Thus the size of the depletion region scales linearly with the channel length, which seems promising for a system on a larger scale as we shall investigate in Chapter 7. In Fig. 5.4(b) we have used Eq. (5.23) to make a plot of the size of the depletion region for different potentials. This is done by claiming

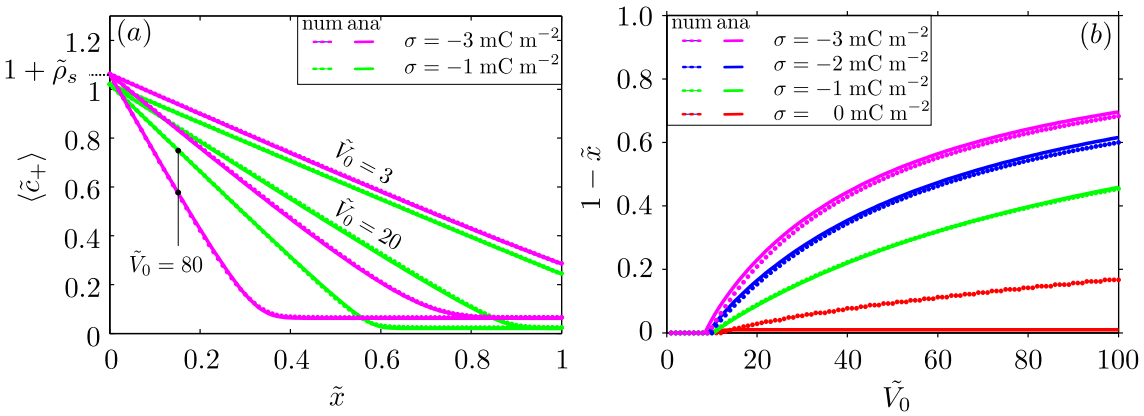

Figure 5.4: Depletion regions for different wall charges. (a) The normalised average cation concentration plotted along the channel. (b) The size of the depletion region is plotted for varying potentials.

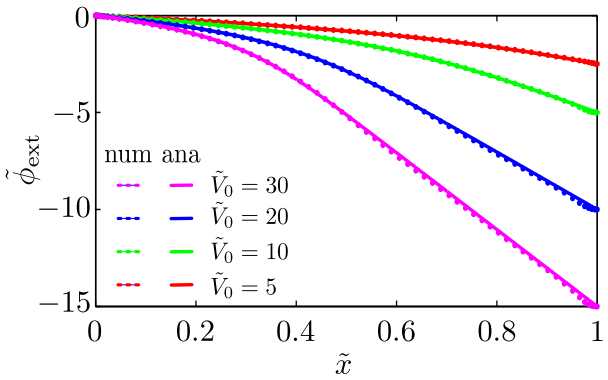

Figure 5.5: Numerical solutions for the normalised external potential compared with the analytical result from Eq. (5.22). The potentials are plotted along the channel for varying external potential drop $\tilde{V}_0$.

$\langle \tilde{c}_+ \rangle + \tilde{\rho}_s$ to be 0.01 in Eq. (5.23) and then plot $1 - \tilde{x}$ as the size of the depletion region. It is seen that, independently of the wall charge, the depletion region starts around $\tilde{V}_0 = 10$ corresponding to where the overlimiting current takes places in Fig. 5.3(b). It is important to emphasize that from Eq. (5.23), the depletion region will occur around $V_0 = 10\, V_\mathrm{T}$ ($5\, V_\mathrm{T}$ from $x = 0$ to $x = L$) independently of the length of the channel. This is confirmed in Chapter 7 where we make a system on a larger scale (see Fig. 7.6).

5.6 Introducing electro-osmotic flow

So far we have only considered a channel with no flow. But in the presence of an electric field, ions will start to move in the electrolyte due to the electrophoretic term in the Nernst-Planck equation, $\boldsymbol{J}_{\pm}^{\text{elec}} = -D_{\pm}c_{\pm}\boldsymbol{\nabla}\tilde{\phi}_{\text{ext}}$. In the Debye layer, where we have more cations than anions, we will have a net flow of particles which by viscous forces give rise to electro-osmotic flow of the fluid surrounding them. As the fluid is blocked by the membrane, a back pressure must be established for the velocity to satisfy the continuity equation $\boldsymbol{\nabla}\cdot\boldsymbol{v} = 0$.

We investigate this electro-osmotic flow in the channel in the presence of an external electric field E in the x-direction. We assume that the plates are long and symmetric so that the velocity field is invariant in the x direction. Using the boundary conditions $v_x(H/2) = v_x(-H/2) = 0$ and $\phi_{\text{eq}}(H/2) = \phi_{\text{eq}}(-H/2) = \zeta$ we find from the Stokes equation in the case of no back pressure,

$$\partial_y^2 v_x(y) + \rho_{\text{el}}E = 0 \quad \Rightarrow \quad v_x(y) = \big(\zeta - \phi_{\text{eq}}(y)\big)\,\frac{\epsilon_{\text{w}}E}{\eta}, \tag{5.24}$$

where we have used the Poisson equation to substitute $\rho_{\text{el}} = -\epsilon_{\text{w}}\partial_y^2\phi_{\text{eq}}$. We use the well known symmetric equilibrium potential for a two plated system

$$\phi_{\text{eq}}(y) = \zeta\frac{\cosh(\frac{y}{\lambda_D})}{\cosh(\frac{H}{2\lambda_D})}, \tag{5.25}$$

satisfying the boundary conditions $\phi_{\text{eq}}(H/2) = \phi_{\text{eq}}(-H/2) = \zeta$ and valid in the Debye-Hückel limit, $|Z|e\phi \ll k_{\text{B}}T$. Inserting Eq. (5.25) into Eq. (5.24) we find the solution,

$$v_x(y) = \left(1 - \frac{\cosh(\frac{y}{\lambda_D})}{\cosh(\frac{H}{2\lambda_D})}\right)\frac{\epsilon_{\text{w}}\zeta}{\eta}E. \tag{5.26}$$

We notice that in the limit $\lambda_{\text{D}} \ll H/2$ the velocity will be almost constant across the channel except for the boundaries of course, where it because of the no-slip constraint goes to zero. We also notice that the velocity is zero everywhere in case of zero wall charge i.e. $\zeta = 0$ as expected. For very narrow channels i.e. $H \approx \lambda_{\text{D}}$ advection of ions is the main contribution to the current, but as the channel gets higher, conduction dominates[5]. Now introducing the membrane into the system, a back pressure comes into the picture and we now write the total velocity by superimposing the two velocity fields from electro-osmosis and the well known Poiseuille flow for a straight channel with walls at $\pm H/2$. The total velocity therefore becomes

$$v_x(y) = \left[\left(1 - \frac{\cosh(\frac{y}{\lambda_D})}{\cosh(\frac{H}{2\lambda_D})}\right)\frac{\epsilon_{\text{w}}\zeta}{\eta}E\right] + \left[\left(\left(\frac{y}{H/2}\right)^2 - 1\right)\frac{H^2}{8\eta}\partial_x p\right]. \tag{5.27}$$

Since the total flow is zero we require the velocity integrated over a vertical cross section to vanish. Thus we integrate Eq. (5.27) from $-H/2$ to $H/2$ and equate with zero to find

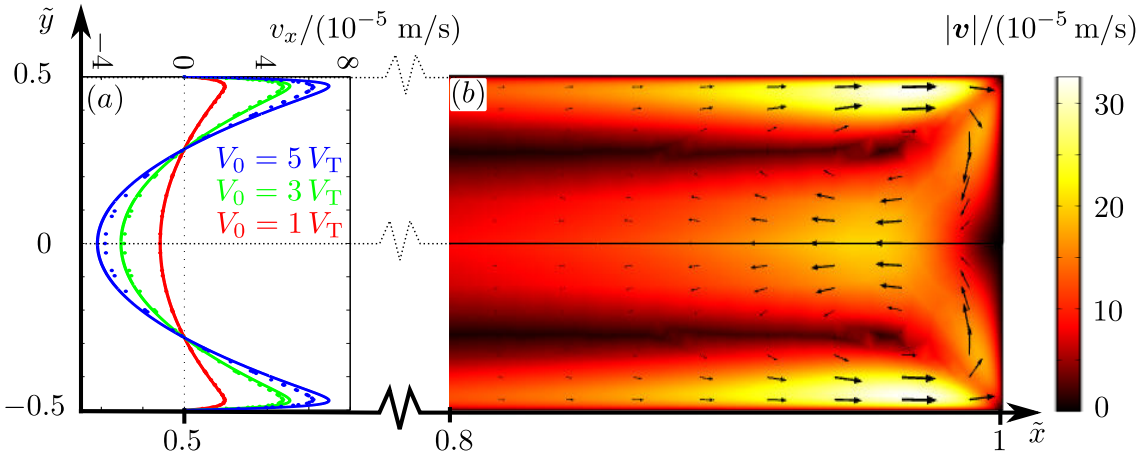

Figure 5.6: (a) Analytical (solid) and numerical (points) solutions for 1D velocity in x-direction plotted along y at $x = L/2$ for three different external potentials. Analytical solution is given by Eq. (5.29) combined with Eq. (5.22). (b) Numerical 2D plot of the velocity in the end of the channel close to the membrane. Colour plot indicates speed and arrows indicate velocity vectors (proportional).

the pressure gradient,

$$\partial_x p = \frac{12}{H^2}\epsilon_w \zeta E \left(1 - \frac{\tanh\left(\frac{H}{2\lambda_D}\right)}{\frac{H}{2\lambda_D}}\right) \approx \frac{12}{H^2}\epsilon_w \zeta E \quad \text{for} \quad H \gg 2\lambda_D. \tag{5.28}$$

Now inserting Eq. (5.28) into Eq. (5.27) gives us the velocity profile for electro-osmosis with back pressure,

$$v_x(y) = \left[-\frac{\cosh\left(\frac{y}{\lambda_D}\right)}{\cosh\left(\frac{H}{2\lambda_D}\right)} - \frac{1}{2} + \left(\frac{y}{H/2}\right)^2\right]\frac{\epsilon_w \zeta}{\eta} E \quad \text{for} \quad H \gg 2\lambda_D. \tag{5.29}$$

The final step is to insert $E = -\partial_x \phi_{ext}$ into Eq. (5.29), using the analytical expression for the external potential from Eq. (5.22). We show the analytical velocity together with numerical solutions in Fig. 5.6(a). The analytical model seems to deviate from the numerical solution for increasing potentials. This corresponds to the somewhat higher current density for the analytical model seen in Fig. 5.3(a). Fig. 5.6(b) shows the 2D velocity. As expected due to high current density at the boundaries (see Fig. 5.3(b)) flow goes to the right at the walls and backwards in the center due to the back pressure.

5.7 Numerical set-up

The solutions given so far have all been analytical. We will now show how to use COMSOL to verify analytical solutions. As described earlier we put in conservation equations. These

Table 5.1: Parameters used in calculations on the microchannel.

Quantity	Label	Value
Height of channel	H	1 μm
Length of channel	L	10 μm
Reservoir Concentration	c_0	1 mM
Cation Diffusion Constant	D_+	1.33×10^{-9} m^2 s^{-1} [5]
Anion Diffusion Constant	D_-	2.03×10^{-9} m^2 s^{-1}[5]
Viscosity of water	η	1 mPa s [5]
Dielectric constant of water	ϵ_{w}	$80.1\,\epsilon_0$[6]
Temperature	T	300 K
Density of water	ρ_{w}	10^3 kg m^{-3}[6]

must be given in weak form along with boundary condition in the form of a constraint or a weak contribution. We shall use the the Stokes equation Eq. (2.7), the continuity equation of mass Eq. (2.2b), the Poisson equation Eq. (2.14a) and the continuity equation of particles Eq. (2.15b).
We will first introduce the governing equations in their weak form and hereafter introduce the boundary conditions.

5.7.1 The Stokes equation

For low Reynold numbers we apply the Stokes equation,

$$0 = \boldsymbol{\nabla} \cdot \boldsymbol{\sigma} + \boldsymbol{f}^{\mathrm{body}}, \tag{5.30}$$

where we remember that $\boldsymbol{\sigma}$ is the viscosity tensor, and we therefore write each element in Eq. (5.30) as

$$0 = \boldsymbol{\nabla} \cdot \boldsymbol{\sigma}_i + f_i^{\mathrm{body}}. \tag{5.31}$$

Multiplying Eq. (5.31) with a test function, integrating by parts and rewriting it by Gauss's Theorem we end up with

$$0 = \int_{\partial\Omega} dA\ \hat{v}_{i,m} \boldsymbol{n} \cdot \boldsymbol{\sigma}_i + \int_{\Omega} dV\ \left[(-\boldsymbol{\nabla} \hat{v}_{i,m}) \cdot \boldsymbol{\sigma}_i + \hat{v}_{i,m} f_i \right], \tag{5.32}$$

which is the equation for the i'th component in the m'th element. The first part describes the flux and Comsol will take $\mathbf{n} \cdot \boldsymbol{\sigma}$ as the input for the Neumann boundary condition. Second part of Eq. (5.32) is the so-called weak form and describes the fluid in the bulk.

5.7.2 The continuity equation

We do not have any continuity equation related explicitly to the pressure. However we can claim that the pressure must settle such as to keep the fluid incompressible. This is done

by multiplying the continuity equation $\boldsymbol{\nabla}\cdot\boldsymbol{v} = 0$ with a test function for the pressure,

$$0 = \int_\Omega dV\ \hat{p}_m \boldsymbol{\nabla}\cdot\boldsymbol{v}, \tag{5.33}$$

where $\hat{p}_m$ is the m'th test function and $\boldsymbol{v}$ is the two dimensional velocity field. Here Eq. (5.33) only describes the pressure in the bulk.

5.7.3 The Poisson equation

We write the poisson equation in the general form from Eq. (2.14a),

$$\boldsymbol{\nabla}\cdot(-\epsilon_\mathrm{w}\boldsymbol{\nabla}\phi_\mathrm{tot}) = \rho_\mathrm{el}. \tag{5.34}$$

We again multiply with a test function, $\hat{\phi}_m$, and integrate by parts

$$\int_{\partial\Omega} dA\ \hat{\phi}_{\mathrm{tot},m}\boldsymbol{n}\cdot(-\epsilon_\mathrm{w}\boldsymbol{\nabla}\phi_\mathrm{tot}) + \int_\Omega dV\ \left[\left(-\boldsymbol{\nabla}\hat{\phi}_{\mathrm{tot},m}\right)\cdot(-\boldsymbol{\nabla}\phi_\mathrm{tot}) - \hat{\phi}_{\mathrm{tot},m}\rho_\mathrm{el}\right] = 0. \tag{5.35}$$

5.7.4 Continuity equation of particles

We model the concentrations by the equation for conservation of ions in Eq. (2.15b). Thus we multiply $\boldsymbol{\nabla}\cdot\boldsymbol{J} = 0$ a testfunction $\hat{c}_\pm$ for the concentrations and write the weak form,

$$\int_{\partial\Omega} dA\ \hat{c_\pm}_{,m}\boldsymbol{n}\cdot\boldsymbol{J}_\pm + \int_\Omega dV\ [(-\boldsymbol{\nabla}\hat{c_\pm}_{,m})\cdot\boldsymbol{J}_\pm] = 0. \tag{5.36}$$

Observe how we for the Stokes equation and the Nernst-Planck equation have two dependent variables, whereas the two other equations only have one. Thus we have 6 equations for each mesh element in our geometry.

5.7.5 Boundary conditions

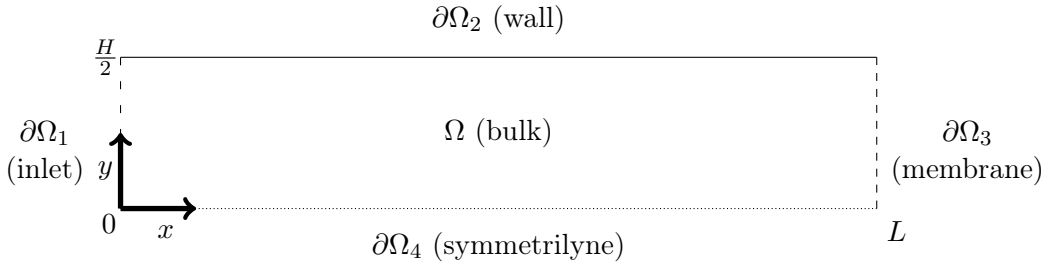

Figure 5.7: Definitions of the four boundaries and the bulk domain.

For clarity we will introduce the boundary conditions for the flow and for the ion movement separately. In Table 5.2 the applied constraints and weak contribution are sumerised. All the weak boundary contributions will be derived and explained in the following. We refer to Fig. 5.7 for a definition of the boundaries.

Flow boundary conditions

Due to the viscosity we require no-slip on the wall which implies a zero velocity Dirichlet constraint for the wall and the membrane.

$$\boldsymbol{v} = \mathbf{0} \quad \text{for} \quad \partial\Omega_2,\, \partial\Omega_3 \tag{5.37}$$

The channel must be long enough for the flow to have established at the left inlet $\partial\Omega_1$, i.e. no change in flow in the x-direction and no flow at all in the vertical direction,

$$\partial_x v_x = 0 \quad \text{for} \quad \partial\Omega_1 \tag{5.38a}$$
$$v_y = 0 \quad \text{for} \quad \partial\Omega_1. \tag{5.38b}$$

To obtain symmetry at the symmetry line there can be no flow across the line and the velocity profile must reach an extremum at the symmetryline.

$$v_y = 0 \quad \text{for} \quad \partial\Omega_4 \tag{5.39a}$$
$$\partial_y v_x = 0 \quad \text{for} \quad \partial\Omega_4. \tag{5.39b}$$

Pressure

We apply a pressure of value $p = p_0$ at the inlet $\partial\Omega_1$. Furthermore due to the wall charge cations will be attracted towards the wall and a pressure gradient in the vertical direction must establish to equalise this attractive force. In order for COMSOL to calculate for the pressure field better we impose a Gouy-Chapman pressure on the constraint of the inlet $\partial\Omega_1$ as follows. By the Stokes equation we have $\boldsymbol{\nabla} p = \rho_{\text{el}}(-\boldsymbol{\nabla}\phi)$. Using the Poisson equation we can write

$$\boldsymbol{\nabla} p = (-\epsilon_{\text{w}}\nabla^2\phi)(-\boldsymbol{\nabla}\phi), \tag{5.40}$$

where ϵ_{w} is assumed constant. Given the general relation $((f')^2)' = 2f'f''$ we have

$$\boldsymbol{\nabla} p = \frac{\epsilon_w}{2}\boldsymbol{\nabla}\left((\boldsymbol{\nabla}\phi)^2\right) \tag{5.41a}$$
$$p = p_0 + \frac{\epsilon_{\text{w}}}{2}(\boldsymbol{\nabla}\phi)^2, \tag{5.41b}$$

satisfying that $\boldsymbol{\nabla}\phi_{\text{eq}}(0,0) = 0$ and $p(0,0) = p_0$. We see that the first term expresses the well known energy density for a electrostatic field[10]. Inserting the Gouy-Chapman potential from Eq. (3.5) we get

$$p(y) = p_0 + V_{\text{T}}|Z|ec_0\left[\frac{\tanh\left(\tilde{\zeta}/4\right)\exp\left(\frac{H/2-y}{\lambda_{\text{D}}}\right)}{1-\tanh\left(\tilde{\zeta}/4\right)\exp\left(\frac{H/2-y}{\lambda_{\text{D}}}\right)}\right]^2 \equiv p_0 + p_{\text{GC}} \quad \text{for} \quad \partial\Omega_1 \tag{5.42}$$

where we have defined p_{GC} as the pressure due to the wall charge. Please notice that in case of no wall charge, $\zeta = 0$ and the pressure will be p_0 at the entire inlet as expected.

Electric Pontential

It appeared easier for COMSOL to converge when the chemical potential was set to zero at the membrane. Therefore we we introduced a potential shift in the calculations, and substituted the results back again, so that the boundary conditions for the electric field are the same as shown in Fig. 5.1.

We use the electrochemical potential to set the boundary condition for the electric potential.

$$\mu_+ = |Z|eV_0 \quad \text{for} \quad \partial\Omega_1 \tag{5.43a}$$

$$\mu_+ = 0 \quad \text{for} \quad \partial\Omega_3. \tag{5.43b}$$

We then set COMSOL to adjust for the potential to satisfy this equation. For the wall we apply the boundary condition,

$$\boldsymbol{n}\cdot(-\epsilon_{\mathrm{w}}\boldsymbol{\nabla}\phi) = -\sigma, \tag{5.44}$$

where $\boldsymbol{n}$ is the normal vector pointing out of the domain.

Ionic concentration

The concentrations can assume both very high numbers at the Debye layer and low numbers at the depletion region. In both cases in appears better for COMSOL to work with the logarithm of the concentration and thus we introduce two new variables in COMSOL,

$$s_\pm = \ln\left(\frac{c_\pm}{c_0}\right). \tag{5.45}$$

These variables are only used in calculations and we always substitute the results back to $c_\pm$.

There is no flow of ions at the wall or at the symmetry line. At the inlet we require the concentration to be c_0 to satisfy the reservoir condition. However the wall charge will perturb this a little. We therefore describe the concentration of ions with the Boltzmann distribution, Eq. (3.2)

$$c_\pm(0, y) = c_0 \exp(\mp\tilde{\phi}_{\mathrm{GC}})(y) \quad \text{for} \quad \partial\Omega_1 \tag{5.46}$$

where $\tilde{\phi}_{\mathrm{GC}})(y)$ is the dimensionless Gouy-Chapmann solution from Eq. (3.5).

The current density for anions is zero everywhere so we apply no flux on every walls. We do not know the cation current density at the membrane exactly. However we know that the cations concentration decrease towards the membrane and reach minimum very near the front of the membrane. Due to high concentration of cations inside the membrane the concentration has a heavy increase just in front of the membrane. We model L as just before the membrane where $\partial c_+ = 0$. Further there is no slip for the velocity so advection is vanishing. Thus we get the boundary constraint on the membrane,

$$\boldsymbol{J}_+ = -c_+ D_+ \boldsymbol{\nabla}\tilde{\phi} \quad \text{for} \quad \partial\Omega_3. \tag{5.47}$$

5.7.6 Summarising all boundary conditions

Table 5.2: List of all boundary conditions for the microchannel.

	Constraint (Dirichlet)	Equation reference	Weak contribution (Neumann)	Equation reference
$\partial\Omega_1$	$\partial_x v_x = 0$	Eq. (5.38a)		
Inlet	$v_y = 0$	Eq. (5.38b)		
	$p = p_0 + p_{\mathrm{GC}}$	Eq. (5.42)		
	$\mu_+ = \lvert Z\rvert eV_0$	Eq. (5.43a)		
	$c_+ = c_0 \exp(-\tilde{\phi}_{\mathrm{GC}})$	Eq. (3.2)		
	$c_- = c_0 \exp(\tilde{\phi}_{\mathrm{GC}})$	Eq. (3.2)		
$\partial\Omega_2$	$\boldsymbol{v} = \mathbf{0}$	Eq. (5.37)	$\mathbf{n}\cdot\boldsymbol{\sigma} = 0$	Eq. (5.32)
Wall			$\boldsymbol{n}\cdot(-\epsilon_{\mathrm{w}}\boldsymbol{\nabla}\phi) = -\sigma$	Eq. (5.44)
$\partial\Omega_3$	$\boldsymbol{v} = \mathbf{0}$	Eq. (5.37)	$\mathbf{n}\cdot\boldsymbol{\sigma} = 0$	Eq. (5.32)
Membrane	$\mu_+ = 0$	Eq. (5.43b)	$\boldsymbol{n}\cdot\boldsymbol{J}_+ = -c_+\partial_x\tilde{\phi}$	Eq. (5.47)
			$\boldsymbol{n}\cdot\boldsymbol{J}_- = 0$	Eq. (5.36)
$\partial\Omega_4$	$\partial_y v_x = 0$	Eq. (5.39a)		
Symmetry	$v_y = 0$	Eq. (5.39b)	$\boldsymbol{n}\cdot(-\epsilon_{\mathrm{w}}\boldsymbol{\nabla}\phi) = 0$	Eq. (5.35)
line				

5.7.7 Concluding remarks

We have in this chapter described a way to model salt depletion in a microchannel with negatively charged walls. Analytical solutions has been compared with numerical solutions and shown good agreement. However the numerical results showed that in the case of no wall charge a charge polarization occurs in front of the membrane giving rise to a small overlimiting current. Thus was not predicted analytically. Introducing wall charges extends the depletion region further and give rise to a larger overlimiting current. For this system we found that a depletion region appears for external potentials around $10\,V_{\mathrm{T}}$ as shown in Fig. 5.4(b). From Fig. 5.3(a) we see that this corresponds to the potential where the overlimiting current takes place. From Fig. 5.3 we also see a larger depletion region and a higher overlimiting current for increasing wall charge. We found from Eq. (5.23) that the size of the depletion region scales with the length of the channel which seems promising for a system on a larger scale as we shall investigate in Chapter 7.

6 | Modeling of porous medium

6.1 Physical modeling of porous medium

In Fig. 6.1(a) we show a sketch of how we model the porous medium as consisting of many small glass beads which we approximate by uniform spheres with diameter d. As shown in Fig. 6.1(b) these beads effectively form many microchannels which we assume have approximately the same properties as the microchannel we described in detail in Chapter 5. The hope is to use our knowledge from Chapter 5 to make an effective averaging over these many channels.

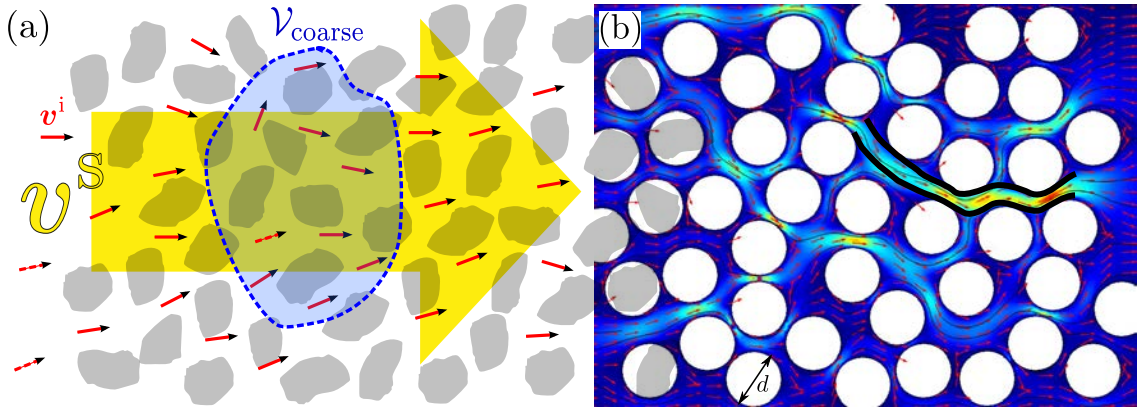

Figure 6.1: Sketch of our physical model of the porous medium as consisting of small beads (grey) which we approximate by uniform spheres with diameter d. We distinguish the *interstitial* velocity $\boldsymbol{v}^{\text{i}}$ (small red arrows) which is the velocity inside the porous medium and the *superficial* velocity $\boldsymbol{v}^{\text{s}}$ (big yellow arrow) which is the velocity averaged over a domain Ω (blue).

In the introduction we explained how the continuum hypothesis gave us the ability to consider variables as fields. In the same way we now formulate a continuum hypothesis for this new model. This time we define fields as the average of fields in many microchannels. Let us keep the same uncertainty of 0.5 % in the number of microchannels so that we need $N = 4 \times 10^4$ channels. Assuming one channel per bead and an average distance between the beads of approximately $1.5\,d = 1.5 \times 10\,\mu$m[17], we need $\mathcal{V}_{\text{coarse}}$ to be about $\mathcal{V}_{\text{coarse}} = Nd^3 \approx (0.5\,\text{mm})^3$ and hence we can only resolve our system in length scales of

0.5 mm. However, for computational reasons we shall use a porous material of an area of about $(1\,\mathrm{mm})^2$ and thus the fields presented in this model is much finer than this coarse grained model allows us.

6.2 Variables in porous medium

Now that we have established a new continuum hypothesis and described how we average variables in our coarse grained model we are ready to define the variables used when dealing with porous medium. We emphasize that all variables presented in this section might be position depended for inhomogeneous porous medium. We also remind the reader that all variables are averaged over a volume $\mathcal{V}_{\text{coarse}}$. But, to avoid cluttered notation we omit both dependencies and averaging, $\langle\cdot\rangle_{\mathcal{V}_{\text{coarse}}}$.

We start by defining three properties of the porous medium. Porosity ε_{p} is the fraction of void V_{void} volume to the total volume V,

$$\varepsilon_{\text{p}} \equiv \frac{V_{\text{void}}}{V}. \tag{6.1}$$

The specific area S is the fraction of surface area A to solids volume $V(1-\varepsilon_{\text{p}})$,

$$S \equiv \frac{A}{V(1-\varepsilon_{\text{p}})}. \tag{6.2}$$

Finally the tortuosity is the fraction of length travelled to the length between the endpoints,

$$\tau \equiv \frac{\text{Length of curve}}{\text{Length of straight line}} \equiv 1.3. \tag{6.3}$$

Please note, that τ might be more complex than just a constant and typically it depends on ε_{p}. However in this thesis we shall use the simple constant 1.3 corresponding to a porosity of around 0.4 according to more comprehensive mathematical studies for spherical particles[18].

As sketched in Fig. 6.1 we distinguish between the interstitial velocity $\boldsymbol{v}^{\text{i}}$ and superficial velocity $\boldsymbol{v}^{\text{s}}$. $\boldsymbol{v}^{\text{i}}$ is the average microscopic in between the channels. $\boldsymbol{v}^{\text{s}}$ is the macroscopic velocity corresponding to an average velocity flowing in the entire volume instead of only in the void volume. If we demand $\boldsymbol{v}^{\text{i}}$ and $\boldsymbol{v}^{\text{s}}$ to give the same flow rate, the relations must be,

$$\boldsymbol{v}^{\text{s}} \equiv \varepsilon_{\text{p}}\boldsymbol{v}^{\text{i}}. \tag{6.4}$$

In the same way, we establish the relations for mass density, ionic concentration and charge density, which can be defined either per *total* volume (superficial) or per *void* volume (interstitial),

$$\rho^{\text{s}} \equiv \varepsilon_{\text{p}}\rho^{\text{i}} \qquad c^{\text{s}}_{\pm} \equiv \varepsilon_{\text{p}}c^{\text{i}}_{\pm} \qquad \rho^{\text{s}}_{\text{el}} \equiv \varepsilon_{\text{p}}\rho^{\text{i}}_{\text{el}}. \tag{6.5}$$

Note that in the presence of a wall charge σ we can define the interstitial charge density as charge per void volume,

$$\rho^{\text{i}}_{\text{el}} \equiv |Z|e(c^{\text{i}}_{+} - c^{\text{i}}_{-}) + \sigma S(1-\varepsilon_{\text{p}})/\varepsilon_{\text{p}}. \tag{6.6}$$

In the rest of this thesis we shall only use interstitial variables i.e. $\boldsymbol{v}^{\mathrm{i}}$, $c^{\mathrm{i}}_{\pm}$, $\rho^{\mathrm{i}}_{\mathrm{el}}$.

6.3 Hydrodynamics in porous medium

In this section we define the continuity equation of mass and the permeability k of the porous medium.

We define the mass current density by the following argument: Imagine a velocity field in the x-direction with velocity v^{i} flowing through many channels and crossing a total area $\Delta y \Delta z$. In the time $\Delta t = \Delta x / v^{\mathrm{i}}$ a volume of $\Delta V \varepsilon_{\mathrm{p}}$ has flown through this area. Then the mass current density must be defined as

$$J_{\mathrm{mass},x} \equiv \frac{\text{mass}}{\text{area} \times \text{time}} = \frac{\rho^{\mathrm{i}}(\Delta V \varepsilon_{\mathrm{p}})}{\Delta y \Delta z \times (\Delta x / v^{\mathrm{i}}_x)} = \rho^{\mathrm{i}} v^{\mathrm{i}} \varepsilon_{\mathrm{p}}. \tag{6.7}$$

By this argument and by Eqs. (6.6) and (6.5) we see that there are many right ways of defining the mass current density,

$$\boldsymbol{J}_{\mathrm{mass}} = \rho^{\mathrm{i}} \boldsymbol{v}^{\mathrm{i}} \varepsilon_{\mathrm{p}} = \rho^{\mathrm{i}} \boldsymbol{v}^{\mathrm{s}} = \rho^{\mathrm{s}} \boldsymbol{v}^{\mathrm{i}}. \tag{6.8}$$

Since we consider water as an incompressible fluid, ρ^{i} is just a constant, $\rho^{\mathrm{i}} = \rho_{\mathrm{w}}$ and we choose the relation with ρ^{i} and $\boldsymbol{v}^{\mathrm{i}}$. Thus the continuity equation Eq. (2.2) for porous medium must be

$$\partial_t \rho^{\mathrm{i}} = -\boldsymbol{\nabla} \cdot (\rho^{\mathrm{i}} \boldsymbol{v}^{\mathrm{i}} \varepsilon_{\mathrm{p}}(\boldsymbol{r})) \tag{6.9a}$$

$$0 = \boldsymbol{\nabla} \cdot \big(\boldsymbol{v}^{\mathrm{i}} \varepsilon_{\mathrm{p}}(\boldsymbol{r})\big) \quad \text{(incompressible fluids)}, \tag{6.9b}$$

where we have emphasized that ε_{p} is a function of $\boldsymbol{r}$ for inhomogeneous media thus must be included in the divergence.

For the porous medium we write the Navier-Stokes with the interstitial velocity,

$$\rho^{\mathrm{i}} \left[\partial_t + \boldsymbol{v}^{\mathrm{i}} \cdot \boldsymbol{\nabla}\right] \boldsymbol{v}^{\mathrm{i}} = -\boldsymbol{\nabla} p + \eta \nabla^2 \boldsymbol{v}^{\mathrm{i}} + \boldsymbol{f}^{\mathrm{body}} - \frac{\eta}{k} \boldsymbol{v}^{\mathrm{i}}, \tag{6.10}$$

where the last term accounts for all viscous drag from the porous medium. The rest of this section serves to determine k in our model.

It is suggested[19] that k should be proportional to the square of the hydraulic diameter d_{hyd}, which is conventionally defined as four times the flows cross-sectional area divided by the wetted perimeter. In our case, we work with porous medium where each pore does not have well defined dimensions. However, we can approximate d_{hyd} using the fraction of void space V_{void} to the surface area A[19],

$$d_{\mathrm{hyd}} = 4 \frac{V_{\mathrm{void}}}{A} = 4 \frac{\varepsilon_{\mathrm{p}}}{S(1 - \varepsilon_{\mathrm{p}})}, \tag{6.11}$$

where we have used Eqs. (6.1) and (6.2) to write d_{hyd} in terms of the more convenient terms S and ε_{p}. We can think of the hydraulic diameter as the diameter of a circular channel should have if it should replace a more complex channel without changing the flow properties significantly. Thus we consider each small domain $\mathcal{V}_{\text{coarse}}$ in the porous medium as replaced by a circular channel with diameter d_{hyd} with the velocity $\boldsymbol{v}^{\text{i}}$ flowing through it.

We choose $k = d_{\text{hyd}}^2/K$ where K is the dimensionless *Kozeny* constant. Just as for τ it is shown that this value might be strongly depended on ε_{p}[20]. However in this model we shall use $K = 5$ suggested by P. C. Carman[19]. Finally we choose $S = 6/d$ for spherical particles with diameter d and arrive at the final value of the permeability,

$$k = \frac{d^2\varepsilon_{\text{p}}^2}{180(1-\varepsilon_{\text{p}})^2}. \tag{6.12}$$

Note that if we had chosen $\boldsymbol{v}^{\text{s}}$ in the Navier Stokes, k should be multiplied by ε_{p}.

6.4 Electrostatics in porous medium

Within electrostatics we make two adjustments in the equations from Section 2.2. The first one concerns the effective electric permittivity of porous medium. There are many approaches on determining this value. A comprehensive study based on thousands of computer simulations was made by Kärkkäinen[21] with the conclusion that one can only tell the most likely effective electric permittivity for a mixture. As a first approach we shall apply the most simple model where we imagine that the porous medium consists of partly glass with permittivity ϵ_{g} and partly water with permittivity ϵ_{w} so that,

$$\epsilon_{\text{eff}} = (1-\varepsilon_{\text{p}})\epsilon_{\text{g}} + \varepsilon_{\text{p}}\epsilon_{\text{w}}. \tag{6.13}$$

Despite the fact that we know from Kärkkäinen that this approach is not exact at all we will however in this first approach only consider a simple model that changes the permittivity in the porous medium relative to the pure water.

The second adjustment concerns the charge density. We account for all surface charge σ on the surface of the glass beads by using the same approach as we did in Chapter 5 i.e. we smear out all the wall charge on the void volume,

$$\rho_{\text{el}}^{\text{i}} = |Z|e(c_+^{\text{i}} - c_-^{\text{i}}) + \frac{S(1-\varepsilon_{\text{p}})}{\varepsilon_{\text{p}}}\sigma. \tag{6.14}$$

6.5 Electrokinetics in porous medium

The ionic current densities in porous medium must be analog to the mass current density from Eq. (6.8)

$$\boldsymbol{J}_{\pm}^{\text{adv}} = c_{\pm}^{\text{i}}\boldsymbol{v}^{\text{i}}\varepsilon_{\text{p}} = c_{\pm}^{\text{i}}\boldsymbol{v}^{\text{s}} = c_{\pm}^{\text{s}}\boldsymbol{v}^{\text{i}}. \tag{6.15}$$

Now, in this model we shall write the first version. Then for the diffusive and electrophoretic part of the ionic currents we keep the concentration as $c_{\pm}^{\text{i}}$. Then we adjust the diffusivities

$D_\pm$ by two factors: we multiply by ε_p since ions only move in the void space, and we divide by τ^2 since ions do not move in straight lines in the porous medium[18]. Thus we write the ionic current densities,

$$\boldsymbol{J}_\pm \equiv c_\pm^\mathrm{i}\boldsymbol{v}^\mathrm{i}\varepsilon_\mathrm{p} - \left(\frac{D_\pm\varepsilon_\mathrm{p}}{\tau^2}\right)\nabla c_\pm^\mathrm{i} \mp \left(\frac{D_\pm\varepsilon_\mathrm{p}}{\tau^2}\right) c_\pm^\mathrm{i}\nabla\tilde{\phi}. \tag{6.16}$$

After redefining the ionic currents, the conservation of particles still apply,

$$\partial_t c_\pm = -\boldsymbol{\nabla}\cdot\boldsymbol{J}_\pm + R \tag{6.17a}$$

$$0 = -\boldsymbol{\nabla}\cdot\boldsymbol{J}_\pm \quad \text{(stady state and no chemical reactions).} \tag{6.17b}$$

6.6 Model overview

In this section we summarize our new definitions in this coarse grained model for porous medium by Table 7.1.

Category	New definition
Coarse resolution	$\approx 0.5\,\mathrm{mm}$ for $d = 10\,\mu\mathrm{m}$
Velocity	$\boldsymbol{v} \to \boldsymbol{v}^\mathrm{i}$
Mass density	$\rho \to \rho^\mathrm{i}$
Charge density	$\rho_\mathrm{el} \to \rho_\mathrm{el}^\mathrm{i}$
Ionic density	$c_\pm \to c_\pm^\mathrm{i}$
Diffusivity	$D_\pm \to \dfrac{D_\pm\varepsilon_\mathrm{p}}{\tau^2}$
Charge density	$\rho_\mathrm{el}^\mathrm{i} = \lvert Z\rvert e(c_+^\mathrm{i} - c_-^\mathrm{i}) + \dfrac{S(1-\varepsilon_\mathrm{p})}{\varepsilon_\mathrm{p}}\sigma$
Permeability	$k = \dfrac{d^2\varepsilon_\mathrm{p}^2}{180(1-\varepsilon_\mathrm{p})^2}$
Permittivity	$\epsilon_\mathrm{eff} = (1-\varepsilon_\mathrm{p})\epsilon_\mathrm{g} + \varepsilon_\mathrm{p}\epsilon_\mathrm{w}$

Table 6.1: List of new definitions made when dealing with porous medium.

7 | Desalination

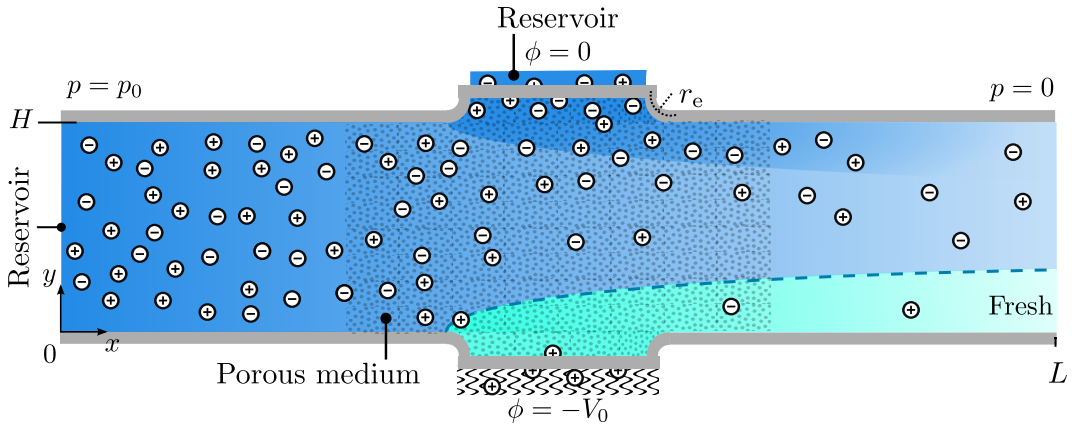

Figure 7.1: Sketch of the channel set-up with height H and length L both in the order of mm. A porous medium is placed in the middle with a cation selective membrane at the bottom and a reservoir at the top. An electric potential drop of V_0 is applied over the porous medium. A pressure drop of p_0 give rise to a flow from the reservoir to the left through the porous medium and out of the outlet to the right.

In Fig. 7.1 we show the set-up for the a new channel in millimetre scale. The idea behind this design is to be able to apply a pressure driven transverse flow to wash out desalinated water. Physically we imagine the porous medium as small glass beads as shown in Fig. 6.1. In this way the porous medium will form small micro channels in all directions. The hope is, that microchannels formed in the vertical direction will act as the microchannel we described in Chapter 5.

Since we only found convergence in COMSOL for a porosity around $\varepsilon_p = 0.4$ we have chosen this fixed value and unfortunately we were not able to investigate the full effect of changing this parameter. However we *were* able to vary the potential, the pressure and the surface charge, revealing some interesting results.

In the following we will handle hydrodynamics and electrodynamics separately for this setup to give an intuition of the complex behavior. Finally we show desalination in the fully coupled system.

7.1 Numerical set-up

Table 7.1: List of parameters used in the channel with porous medium.

Quantity	Label	Value
Length of channel	L	15 mm
Height of channel	H	3 mm
Width of porous medium	W_m	6 mm
Width of membrane	W_p	6 mm
Height of extensions	d_e	0.1 mm
Mean bead diameter	d	10 μm
Porosity	ε_p	0.4
Tortuosity	τ	1.3

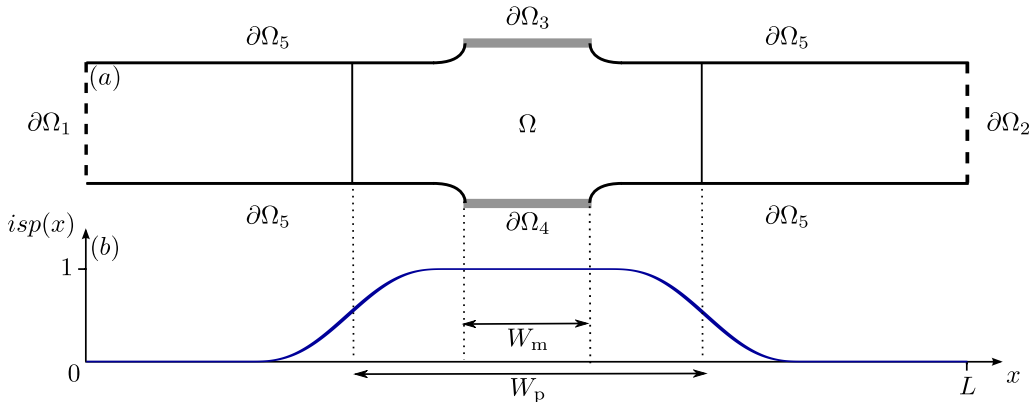

Figure 7.2: (a) Boundaries and bulk notations for channel with porous medium. (b) 1D plot of the $isp(x)$ function used to describe the variations of the porosity.

7.1.1 Design of geometry

As shown in Fig. 7.2 we implement the porous medium by defining a second derivative continuous step function $isp(x)$ (is porous) with a relative transition length of 0.3, i.e. the transition length is $0.3\ (L - W_\mathrm{p})/2 + 0.3\ W_\mathrm{p}$. Then the porosity is $\varepsilon_\mathrm{p} \equiv 0.4\ isp(x)$.

Another numerical implementation in the design is the small extensions of height $d_\mathrm{e} = 0.1$ mm near the membrane and the top reservoir. They serve to avoid discontinuous boundary conditions near the membrane. At the wall we have no flux on the electric field

$$\boldsymbol{n}\cdot(\boldsymbol{\nabla}\phi) = 0, \tag{7.1}$$

since we assume charge neutrality in the porous medium so that there is no net charge inside the porous medium to form a flux in the electric field out of the channel. At the

membrane and top reservoir on the other hand we have a Dirichlet boundary condition. Without these extensions we have seen huge charge densities just at the boundary between the wall and the membrane giving rise to a huge tangential electric force on the fluid.

7.1.2 Boundary conditions for hydrodynamics

For the flow we apply the usual no slip boundary conditions on the walls, $\boldsymbol{v}^{\mathrm{i}} = 0$. Further we assume transverse invariance in the flow at the left inlet and the outlet so that $\partial_x v_x^{\mathrm{i}} = 0$ and $v_y^{\mathrm{i}} = 0$. We set the pressure to

$$p = p_0 \qquad \text{for} \quad \partial\Omega_1 \tag{7.2a}$$
$$p = 0 \qquad \text{for} \quad \partial\Omega_2. \tag{7.2b}$$

at the left inlet and at the outlet, respectively.

7.1.3 Boundary conditions for electrodynamics

Since there is a build in space charge of $S(1-\varepsilon_{\mathrm{p}})\sigma$, we set the concentration at the center inlet to

$$c_+^{\mathrm{i}} = c_0 - \sigma S(1-\varepsilon_{\mathrm{p}})/e \qquad \text{for} \quad \partial\Omega_3 \tag{7.3a}$$
$$c_-^{\mathrm{i}} = c_0 \qquad \text{for} \quad \partial\Omega_3, \tag{7.3b}$$

and at the left inlet,

$$c_\pm^{\mathrm{i}} = c_0 \quad \text{for} \quad \partial\Omega_1 \tag{7.4}$$

Then at the outlet we again assume transverse invariance of the concentrations,

$$\partial_x c_\pm^{\mathrm{i}} = 0 \quad \text{for} \quad \partial\Omega_2. \tag{7.5}$$

By Eq. (7.5) there is no diffusion at the outlet and since the outlet is far away from the electrodes we claim that the currents just follow the flow,

$$\boldsymbol{n}\cdot\boldsymbol{J}_\pm = c_\pm^{\mathrm{i}} v_x^{\mathrm{i}} \quad \text{for} \quad \partial\Omega_2. \tag{7.6}$$

The electrical potential drop from the center inlet to the membrane is V_0 and we require the following constraints

$$\phi = 0 \quad \text{for} \quad \partial\Omega_3, \tag{7.7a}$$
$$\phi = -V_0 \quad \text{for} \quad \partial\Omega_4. \tag{7.7b}$$
$$\tag{7.7c}$$

Finally we model the membrane the same way as in Chapter 5 except for a small change in the diffusivity,

$$\boldsymbol{n}\cdot\boldsymbol{J}_+ = -(D_+\varepsilon_{\mathrm{p}}/\tau^2)c_+^{\mathrm{i}}\nabla\phi \quad \text{for} \quad \partial\Omega_4. \tag{7.8}$$

All boundary condition are shown in Table 7.2.

Table 7.2: List of boundary conditions for the macro model channel.

	Constraint (Dirichlet)	Eq. Ref.	Weak contribution (Neumann)	Eq. Ref.
Ω_1 (left inlet)	$v_y^{\mathrm{i}} = 0$	Eq. (5.38b)	$\boldsymbol{n}\cdot\boldsymbol{E} = 0$	Eq. (7.1)
	$\partial_x v_x^{\mathrm{i}} = 0$	Eq. (5.38a)		
	$p = p_0$	Eq. (7.2a)		
	$c_{\pm}^{\mathrm{i}} = c_0$	Eq. (7.4)		
Ω_2 (outlet)	$v_y^{\mathrm{i}} = 0$	Eq. (5.38b)	$\boldsymbol{n}\cdot\boldsymbol{J}_{\pm} = c_{\pm}^{\mathrm{i}} v_x^{\mathrm{i}}$	Eq. (7.6)
	$\partial_x v_x^{\mathrm{i}} = 0$	Eq. (5.38a)	$\boldsymbol{n}\cdot\boldsymbol{E} = 0$	Eq. (7.1)
	$\partial_x c_{\pm}^{\mathrm{i}} = 0$	Eq. (7.5)		
	$p = 0$	Eq. (7.2b)		
Ω_3 (center inlet)	$\boldsymbol{v}^{\mathrm{i}} = \boldsymbol{0}$	Eq. (5.37)		
	$c_+^{\mathrm{i}} = c_0 - \sigma S(1-\varepsilon_{\mathrm{p}})/e$	Eq. (7.3a)		
	$c_-^{\mathrm{i}} = c_0$	Eq. (7.7b)		
	$\phi = 0$	Eq. (7.7a)		
Ω_4 (membrane)	$\boldsymbol{v}^{\mathrm{i}} = \boldsymbol{0}$	Eq. (5.37)	$\boldsymbol{n}\cdot\boldsymbol{J}_- = 0$	Eq. (5.36)
	$\phi = -V_0$	Eq. (7.7a)	$\boldsymbol{n}\cdot\boldsymbol{J}_+ = -(D_+\varepsilon_{\mathrm{p}}/\tau^2)c_+^{\mathrm{i}}\nabla\phi$	Eq. (7.8)
Ω_5(walls)	$\boldsymbol{v}^{\mathrm{i}} = \boldsymbol{0}$	Eq. (5.37)	$\boldsymbol{n}\cdot\boldsymbol{E} = 0$	Eq. (7.1)

7.2 Illustration of pressure driven flow in porous medium

We investigate a channel of length L and height H with both a porous and void regions as shown in Fig. 7.3. The pressure gradients in the two regions are $\partial_x p_{\mathrm{porous}}$ and $\partial_x p_{\mathrm{void}}$ respectively. By solving the Stokes equation in the two regions we get the flow rate in one dimension as $Q = \int_0^H \mathrm{d}y\, v$,

$$0 = -\partial_x p_{\mathrm{void}} + \eta\partial_y^2 v_{\mathrm{void}} \quad \rightarrow \quad Q_{\mathrm{void}} = -\frac{H^2}{12}\frac{\partial_x p_{\mathrm{void}}}{\eta}H, \tag{7.9a}$$

$$0 = -\partial_x p_{\mathrm{por}} + \eta\partial_y^2 v_{\mathrm{por}} - \frac{\eta}{k}v_{\mathrm{por}} \quad \rightarrow \quad Q_{\mathrm{por}} = -k\left(1 - \frac{\tanh\alpha}{\alpha}\right)\frac{\partial_x p_{\mathrm{por}}}{\eta}H, \tag{7.9b}$$

where we have introduced the dimensionless $\alpha = H/(2\sqrt{k})$. We demand the same flow rate in the porous medium as in the void region so that

$$\frac{\partial_x p_{\mathrm{por}}}{\partial_x p_{\mathrm{void}}} = \frac{\alpha^2}{3}\left(1 - \frac{\tanh\alpha}{\alpha}\right)^{-1} > \left(\frac{H}{25\,d}\right)^2 \quad \text{for} \quad \varepsilon_{\mathrm{p}} < 0.99. \tag{7.10}$$

In the last step we have inserted k from Eq. (6.12). Since $H \gg 25\,d$ we see that the pressure gradient is much higher in the porous medium. This corresponds to the numerical results shown in Fig. 7.3 where we have also plotted the velocity profiles $\boldsymbol{v}^{\mathrm{s}}$ and $\boldsymbol{v}^{\mathrm{i}}$. Please note how the interstitial velocity is much faster than the superficial velocity inside the porous medium.

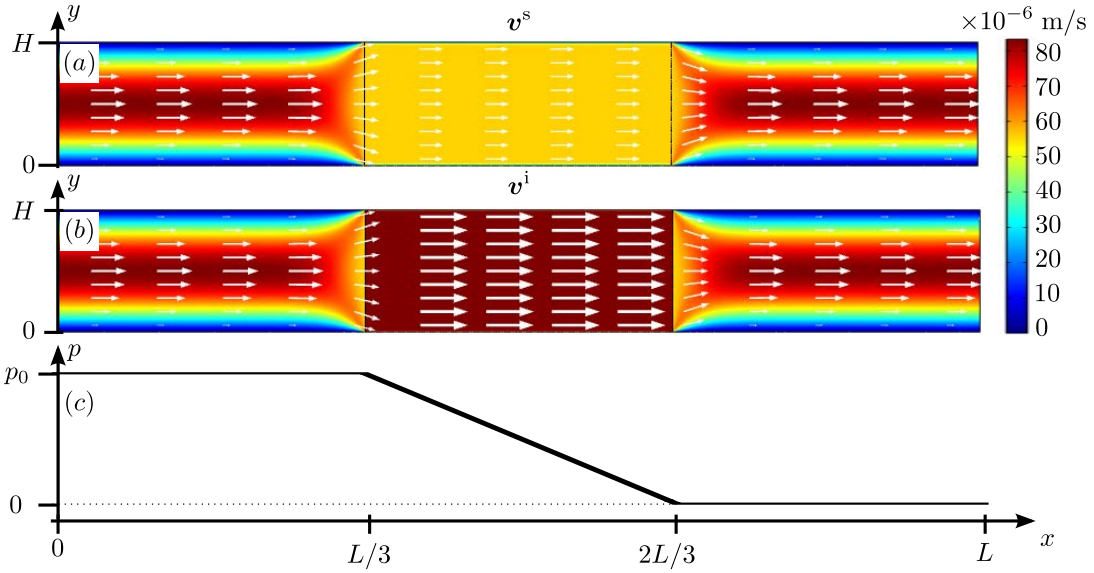

Figure 7.3: A channel with $H = 2$ mm and $L = 15$ mm with porous medium ($\varepsilon_{\mathrm{p}} = 0.4$) from $L/3$ to $2L/3$ and a pressure drop of $p_0 = 1$ kPa. (a) and (b) shows $\boldsymbol{v}^{\mathrm{s}}$ and $\boldsymbol{v}^{\mathrm{i}}$ respectively. (c) shows the pressure through the channel.

7.3 Electrodynamics in porous medium

In this section we will describe how ions behave in the system with no applied pressure drop, $p_0 = 0$. The basis for our electrodynamic analysis will be from Fig. 7.4 showing four 2D-plots of different fields. Considering electrodynamics with no flow is of course important in order to understand the impact of the electrical field alone but it also works as an important test of the numerical model in COMSOL. For a pressure driven flow the advection in the Nernst-Planck equation dominates the diffusion and electrophoresis and so that we will not be able to see the effect from the electric potential alone.

7.3.1 Qualitative 2D analyse

The colors in Fig. 7.4(a) indicates the size of the electrical potential. It is almost constant throughout the whole channel except in front of the membrane. The arrows plot the electrophoresis term from the Nernst-Planck equation and are thus proportional with the electric field. As expected the arrows look like the electric field inside a capacitor.
In Fig. 7.4(b) we plot the cation diffusion vectors and the cation concentration. Like we saw for the microchannel a low cation concentration in front of the membrane will be created. This leads to a diffusion towards the membrane for cations coming from the two reservoirs.
Fig. 7.4(c) plots cation advection vectors and the value of the pressure. We see that advection is vanishing in front of the membrane. This is the same as we saw for the microchannel where the net flow over the channel was zero. Please that the velocity $\boldsymbol{v}^{\mathrm{i}}$

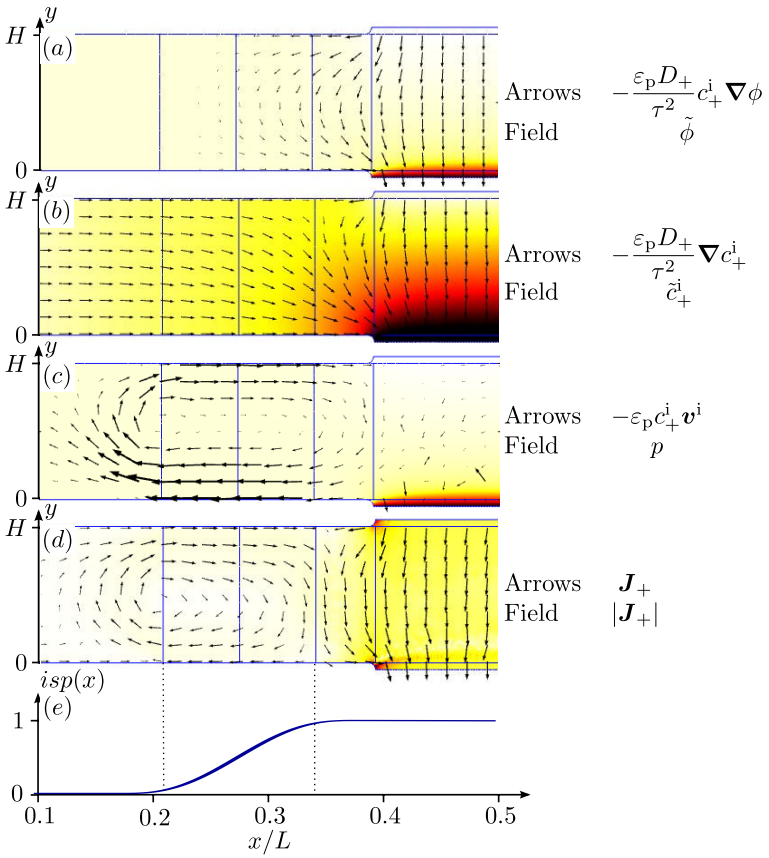

Figure 7.4: Arrows in (a) to (c) show the three terms in the Nernst-Planck equation respectively. (d) shows the full cation current density. All four plots are for $\sigma = -5$ mC/m^2 and $V_0 = 20\ V_T$. White to black indicates the following, (a) $\tilde{\phi} = 0$ to $\tilde{\phi} = -\tilde{V}_0$, (b) $c_+^i = c_0$ to $c_+^i = 0$, (c) $p = 0.9$ kPa to $p = 0$, and (d) high to low current. (e) The $isp(x)$ function is plotted to indicate the transition region in the 2D plots.

is the average interstitial velocity which is zero as expected. As the electro-osmotic back pressure in the microchannel gave a flow straight backwards, now we see that the electro-osmotic backpressure give rise to a flow near the lower walls. This creates a vortex around the porous transition area, so that the velocity is downwards in the porous medium and upwards before the porous medium.

Superimposing the three arrow plots from (a), (b), and (c) in Fig. 7.4 gives us the total cation current, plotted in (d). As one would expect the cation current goes from the reservoir at $\partial\Omega_3$ to the membrane in straight lines following the diffusion and electrophoresis. We also see the effect from the advection term expressed in the vortex around the porous transition area.

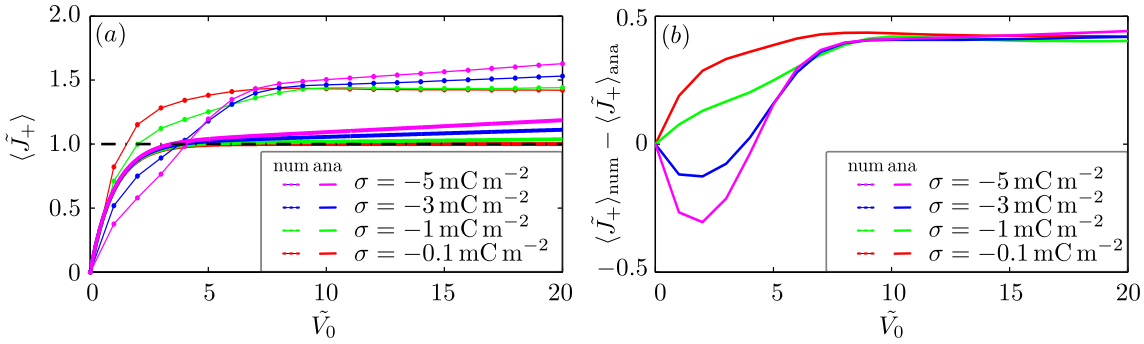

Figure 7.5: The cation current density is normalised given in Eq. (7.12) and the potential is normalised to V_{T} as usually. (a) Average cation current densities plotted versus potential for different wall charges, with both numerical and analytical solutions. Please notice that numerical solutions has been connected by line for better overview and should not be confused with the analytical results. (b) Difference in analytical and numerical results from (a).

7.3.2 Transition function considerations

Fig. 7.2(b) plots the function $isp(x)$ described at the beginning of this chapter. Different relative transitions length have been tested before the choice of 0.3 was taken. A much longer relative transition region is not possible as this would start to remove the porous media in between the two transitions. Making the transition smaller creates of large gradients in the fields, making it difficult for COMSOL to converge. The convergent problem could have been solved by using a much finer mesh at the transition region (a finer mesh at the transition region than the the rest of the bulk has already been implemented) instead of making a larger transition region. This however increases the computational time dramatically and since there are no crucial physical contradictions in using a large transition this was preferred.

7.3.3 Overlimiting current and depletion

The homogeneous cation current field in Fig. 7.4 suggests that we can treat this part of the channel as many small microchannel analogue the microchannel in Chapter 5. We naively assume the Nernst-Planck model from Eq. (5.21a). Now given different boundary conditions and a different $\tilde{\rho}_{\mathrm{s}}$ as suggested in Chapter 6, Eq. (5.21b) changes to

$$\langle \tilde{J}_+ \rangle = 1 - \exp(-\tilde{V}_0) - \frac{\sigma S(1-\varepsilon_{\mathrm{p}})}{|Z|ec_0}\tilde{V}_0, \tag{7.11}$$

where $\langle \tilde{J}_+ \rangle$ due to new geometry and porous media now is defined in the following way

$$\langle \tilde{J}_+ \rangle = \frac{(H+2d_{\mathrm{e}})}{2\left(\frac{D_+\varepsilon_{\mathrm{p}}}{\tau^2}\right)c_0}\langle J_+ \rangle. \tag{7.12}$$

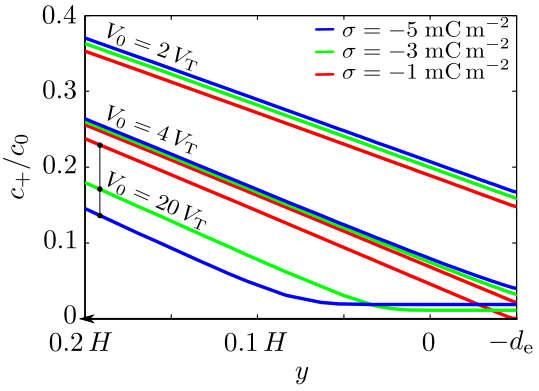

Figure 7.6: Numerical results for the normalised cation concentration in front of the membrane at $x = L/2$ for $p_0 = 0$. Electric potentials and wall charges are varied. The membrane is placed at $-d_e$.

The prefactor in Eq. (7.11) can be understood as the new limiting current. However due to the complex geometry we can no longer expect the diffusion length to be $(H + 2d_e)$ since ions comes from two reservoirs. We have plottedEq. (7.11) together with the numerical results in Fig. 7.5(a) showing a significant difference. However we still notice the behavior of overlimiting current for the numerical results. From Fig. 7.5(b) we see that in the overlmiting current regime the difference between analytical and numerical results are the same constant. This suggests that the limiting current can be expressed just as the prefactor in Eq. (7.11) but with an extra factor depending on the geometry of the system. This is also suggested by Deng et. al and confirmed with experimental results[4]. As expected we see a constant current for no wall charge (red curve). Notice that we were not able to get convergence in the case of $\sigma = 0$ mC m^{-2}, so we have chosen $\sigma = 0.1$ mC m^{-2} instead.

In Chapter 5 we discussed how the depletion region arises at $V_0 = 5V_T$, independent of the wall charge. This behavior is repeated for the macroscopic model as seen in Fig. 7.6 where we confirm depletion at $V_0 = 5V_T$. We refer to Fig. 5.4(a) for a comparison with the results from the micro channel. When the depletion regime is reached higher wall charge causes a larger depletion area which is clearly seen by comparing $\sigma = -5$ mC/m^2 with $\sigma = -3$ mC/m^2 and $\sigma = -1$ mC/m^2 for $V_0 = 20\ V_T$.

7.4 The coupled system

We now combine the models of electrodynamics and hydrodynamics and we end up with our final model for desalination. For the case of no pressure we we see a depletion region just as for the microchannel. But when transverse pressure driven flow is introduced, this flushes out the depletion region so that a larger potential drop is needed to form depletion. The supply of new ions from the flow allows for a higher current through the membrane since the concentration of ions gets closer to c_0.
In figure Fig. 7.7(a) we show the numeric result of the average cation current through the

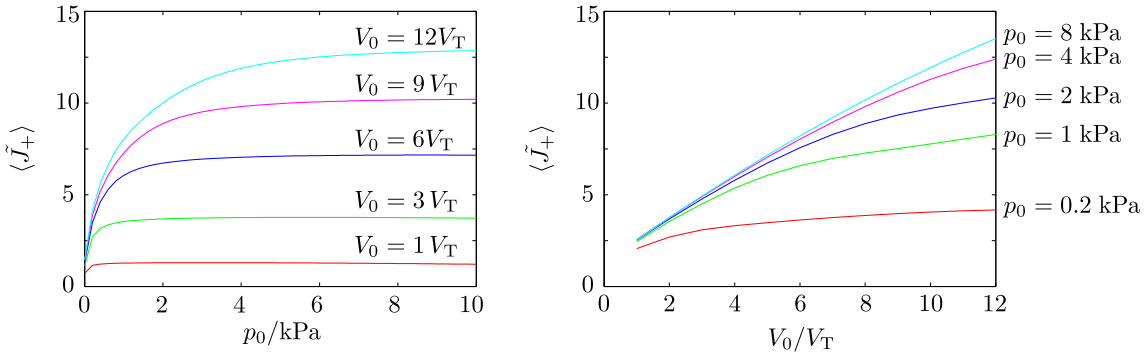

Figure 7.7: The average cation current normalised, in accordance to Eq. (7.12), is plotted. (a) The current plotted versus the pressure for varying potential. (b) The current plotted versus the electrical potential for varying pressure. Both plots are for $\sigma = -1$ mC/m^2.

membrane as a function of pressure and for different potentials. We see that the curves flattens out for high potential as a concentration near c_0 is reached in front of the membrane. This suggests that to a given potential drop a saturation pressure can be found which supplies the area in front of the membrane with a concentration close to c_0. As expected, a larger potential drop gives a higher current. And to a higher potential corresponds a higher saturation pressure.
Fig. 7.7(b) confirms that the saturation point increases with increasing potential. Comparing the IV-curves of Fig. 7.5(a) and Fig. 7.7(b) we find that that an increasing pressure increases the current through the membrane. This can be explained by the steady supply of ions from the flow keeping a higher concentration near the membrane.

In Fig. 7.8(a) we plot the potential across the channel at $x = L/2$ for different pressures. It is seen that the potential approaches a linear drop as the pressure is increased. Since the linear potential is the solution to the Laplace equation, this behavior can be interpreted as the flow flushing out any charge density leaving $\rho_{\text{el}} = 0$ in front of the membrane. In Fig. 7.8(b) we show that the transverse flow ruins the depletion and leaves the area in front of the membrane with a concentration close to c_0.

For high pressures, we therefore suggest a linear potential as shown in Fig. 7.8(a) and a concentration close c_0 in front of the membrane according to Fig. 7.8(b). In this case, since the current through the membrane is only electrophoretic, we can calculate the current as

$$\langle \tilde{J}_+ \rangle = \frac{\tilde{V}_0}{2} \quad \text{(for the saturation pressure, simple model).} \tag{7.13}$$

As seen from figure Fig. 7.7(a) this estimation is too low corresponding to the fact that the limiting current for our system is larger than for the microchannel.

For a desalination device we want to know how effectively we remove ions from the solvent. We are not interested in moving cations from center inlet to the membrane as this

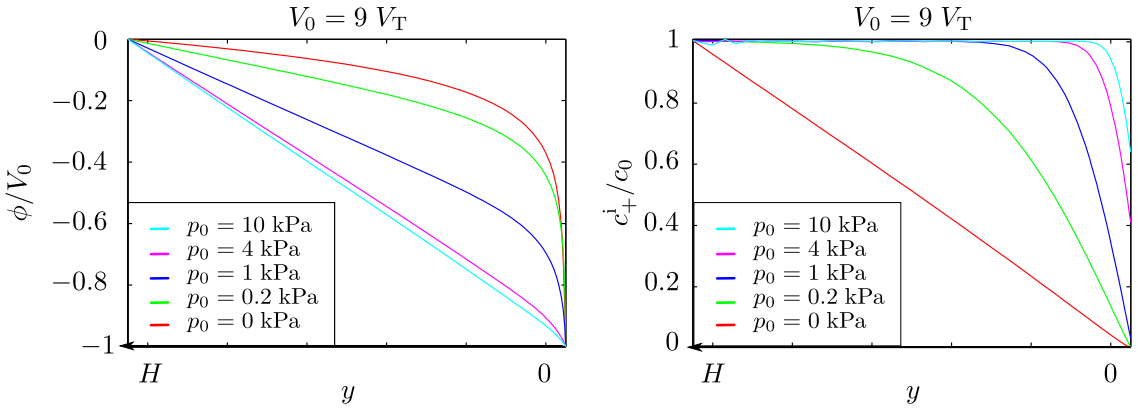

Figure 7.8: Both plots are for $V_0 = 9\ V_T$ and $\sigma = -1\ \mathrm{mC\,m^{-2}}$, plotted across the channel at $x = \frac{L}{2}$ for varying pressure. (a) The normalised electrical potential and (b) the normalised cation concentration.

leads to no real removal of ions from the water. From Fig. 7.7(a) we see that for low pressure the current is much lower than for high pressure. Since the potential is hold constant assume that the increasing cation current is a result of the increasing amount of cations coming from the reservoir at the left inlet. For high efficiency of a desalination device we are interested in increasing the pressure in order to remove ions but not higher than the saturation point. At this point increasing the pressure will not lead to a significant amount of removed ions but the extra ions will rather be flushed right through the channel instead. Considering the potentials from $V_0 = 1\,V_T$ to $V_0 = 9\,V_T$ in Fig. 7.7(a) we set the saturation point to arround $V_0 = 4\ V_T$. In Fig. 7.7(b) wee see that for pressures above $p_0 = 4$ kPa the current depends almost linearly on the potentials in the regime $V_0 = 1\,V_T$ to $V_0 = 12\,V_T$.

We have in Fig. 7.9 have plotted the concentration of cations in the entire channel. For (a) no pressure is applied and a large depletion region is created in front of the membrane. For (b) a pressure of 0.8 kPa is applied. As expected most of the channel has a cation concentration equal to the concentration in reservoir due to flow. However we notice a depletion area close to the membrane and to the right. In a real set-up we suggest to put a separate outlet close to the membrane which would work as to sort out the desalinated water from this area fluid. We compare Fig. 7.9 to Fig. 7.8(b) and notice how an increasing pressure creates a smaller depletion region and a concentration close to c_0. No studies have been carried out for the design and size of a separate outlet channel.

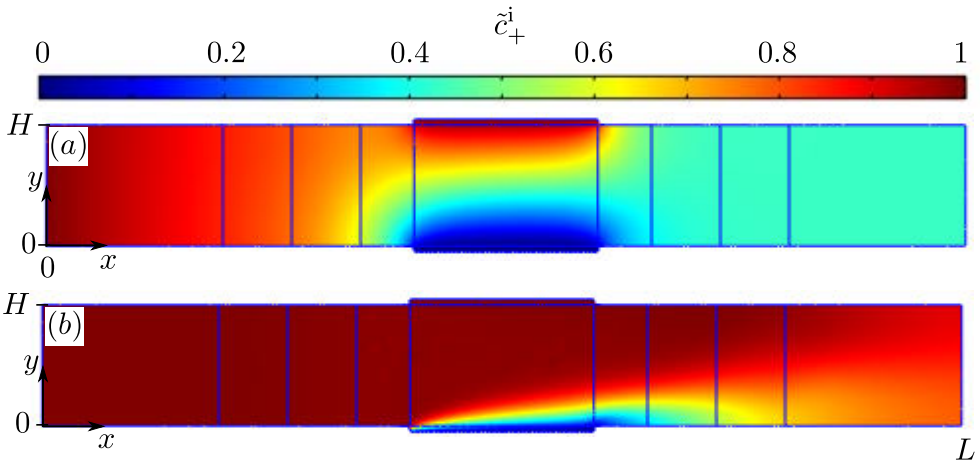

Figure 7.9: 2D plots of the normalised cation concentration for $\sigma = -5\mathrm{mC\ m^{-2}}$. (a) No pressure is applied. (b) For $p_0 = 0.8\,\mathrm{kPa}$.

8 | Conclusion and outlook

We have described the well known behavior of an electrolyte near a charged wall where counter-ions are attracted to the wall giving rise a screening layer near the wall. A microchannel with a cation selective membrane was investigated with and without negatively charged walls. We found that for charged walls, the screening layer acts to conduct a current of cations near the wall giving rise to an overlimiting current. The extended current density near the wall results in a salt depletion region in the bulk in front of the membrane for potential drops above $5\,V_{\mathrm{T}}$. It was shown that the relative size of the depletion region depends on the external potential and the wall charge but *not* on the length of the channel. These results were shown analytically and confirmed by numerical results.

In order to apply the behaviors from the microchannel on a larger scale, we have developed a physical model for a channel containing porous medium by adjusting the governing equations for flow and electrokinetics with parameters characterising porous medium i.e. porosity, tortuosity, and specific area. Based on the approach suggested by Dydek et al.[3] where surface charged is smeared out in the liquid, we model surface charge on the walls of porous medium as an intrinsic volume charge. Claiming an intrinsic volume charge in the porous medium, the system exhibits some of the same behaviors as for the microchannel. Hence we have confirmed the occurrence of a depletion region for potentials above $5\,V_{\mathrm{T}}$ as for the microchannel. In this regime we also showed an overlimiting current for charged walls and a clear limited current for porous medium without wall charge. There are good evidence that the limiting current takes the same form as for a microchannel which is also suggested by Deng et al.[4]. However, due to the more complex geometry of our device we were not able to derive an analytical expression for the limiting current as we did for the microchannel.

Introducing a transverse pressure driven flow in our device in order to flush out desalinated water gave some interesting results. In this case the depleted region in front of the membrane is supplied with new ions from the flow keeping a higher concentration in front of the membrane. We found that for a given potential a certain pressure saturates the area in front of the membrane so that a new, larger limiting current through the membrane is possible. Thus, based on numerical results, we suggest that there should be a most efficient pressure for a given electric potential in order to remove ions from the system.

The model suggested revealed many interesting behaviours and we have only sketched

a few of them. As mentioned, the geometry of our model limits the analytic approach. Despite the fact that we found many of our results physically likely, there are still many cases that we can not simulate, e.g. we found that only some certain values for the porosity gave convergence in COMSOL. For further investigations we suggest to understand the impact from the implementation of porosity by looking at a much simpler system e.g. a straight channel with no flow. One could be even more diligent and investigate electrokinetic behaviour between glass beads to validate the averaging approach suggested in this thesis. Further, understanding the supply of ions from the flow and its exact impact on the overlimiting current better would be vital in developing a device like the one been suggested in this thesis.

Bibliography

[1] U.S. Geological Survey, http://www.usgs.gov, 2014.06.10.

[2] C. P. Nielsen, *Theory and simulation of electrokinetics in micro- and nanochannels*. Master thesis, Technical University of Denmark, http://www.fysik.dtu.dk/microfluidics (2012).

[3] E. V. Dydek, B. Zaltzman, I. Rubinstein, D. S. Deng, A. Mani, and M. Z. Bazant, *Overlimiting current in a microchannel*. Phys Rev Lett **107**(11), 118301 (2011).

[4] M. Z. B. Daosheng Deng, E. Victoria Dydek, *Overlimiting current and shock electrodialysis in porous media*. Langmuir **52**(29), 16167–16177 (2013).

[5] H. Bruus, *Theoretical microfluidics*. No. 18 in Oxford master series in physics (Oxford University Press, Oxford) (2008).

[6] W. M. Haynes, *CRC handbook of chemistry and physics : a ready-reference book of chemical and physical data* (2013).

[7] The Groundwater Foundation, http://www.groundwater.org, 2014.06.11.

[8] I. A. Dickson and C. Goyet, *Handbook of methods for the analysis of the various parameters of thecarbond dioxide system in sea water* (DOE) (1994).

[9] C. Kittel and H. Kroemer, *Thermal Physics, 2. edition* (W. H. Freeman and Company) (1980).

[10] D. J. Griffiths, *Introduction to Electrodynamics, 3. Edition* (Pearson Education, Inc.) (2008).

[11] I. Iranmanesh, R. Barnkob, H. Bruus, and M. Wiklund, *Tunable-angle wedge transducer for improved acoustophoretic control in a microfluidic chip*. Journal of micromichanics and microengineering **23**(10) (2013).

[12] M. W. H. Ley, *Hydrodynamic interactions in microfluidic acoustophoresis*. Master's thesis, DTU Physics, Technical University of Denmark, supervised by Professor Henrik Bruus. (2014).

[13] C. Nielsen, *Introduction to weak form modeling in comsol*. Note on weak form and COMSOL implementation. version 1.3. (2003).

[14] P. B. Muller, R. Barnkob, M. J. H. Jensen, and H. Bruus, *A numerical study of microparticle acoustophoresis driven by acoustic radiation forces and streaming-induced drag forces*. Lab Chip, http://www.fysik.dtu.dk/microfluidics. **22**(12), 4617–4627 (2012).

[15] X. Z. Cheng Fang, Bingliang Wu, *Nafion membrane electrophoresis with direct and simplified end-column pulse electrochemical detection of amino acids*. Electrophoresis **25**(2), 375–380 (2004).

[16] N. Walldorf, *Electrokinetics in Microchannels with Ion-selective Membranes*. B.Sc. thesis, Technical University of Denmark, http://www.fysik.dtu.dk/microfluidics (2014).

[17] PolyScience Inc., http://www.polysciences.com, 2014.06.07.

[18] C. J. Gommes, *Practical methods for measuring the tortuosity of porous materials from binary or gray-tone tomographic reconstructions*. AIChE Journal **55**(8), 2000–2012 (2009).

[19] R. F. Probstein, *Physicochemical hydrodynamics: an introduction* (Wiley-Interscience) (1994).

[20] X. Chen and T. Papathanasiou, *On the variability of the kozeny constant for saturated flow accross unidirectional disordered fiber arrays*. ELSEVIER **37**(6), 836–846 (2006).

[21] K. Karkkainen, *Effective permittivity of mixtures: Numerical validation by the fdtd method*. IEEE Transactions on Geoscience and Remote Sensing **38**(3), 1303–1308 (2000).